

**Global climate
simulations at 3000
year intervals**

J. R. Alder and
S. W. Hostetler

Global climate simulations at 3000 year intervals for the last 21 000 years with the GENMOM coupled atmosphere–ocean model

J. R. Alder and S. W. Hostetler

US Geological Survey, College of Earth, Ocean and Atmospheric Sciences, Oregon State University, Corvallis, Oregon 97331, USA

Received: 13 June 2014 – Accepted: 1 July 2014 – Published: 23 July 2014

Correspondence to: J. R. Alder (jalder@usgs.gov)

Published by Copernicus Publications on behalf of the European Geosciences Union.

Title Page

Abstract

Introduction

Conclusions

References

Tables

Figures



Back

Close

Full Screen / Esc

Printer-friendly Version

Interactive Discussion



Abstract

We apply GENMOM, a coupled atmosphere–ocean climate model, to simulate eight equilibrium “time-segments” at 3000 yr intervals for the past 21 000 years forced by changes in Earth–Sun geometry, atmospheric greenhouse gases (GHGs), continental ice sheets and sea level. Simulated global cooling during the Last Glacial Maximum (LGM) is 3.8 °C and the rate of post-glacial warming is in overall agreement with recently published temperature reconstructions. The greatest rate of warming occurs between 15 and 12 ka (2.4 °C over land, 0.7 °C over oceans and 1.4 °C globally) in response to changes in radiative forcing from the diminished extent of the Northern Hemisphere (NH) ice sheets and increases in GHGs and NH summer insolation. The modeled LGM and 6 ka temperature and precipitation climatologies are generally consistent with proxy reconstructions, the PMIP2 and PMIP3 simulations, and other paleoclimate data-model analyses. The model does not capture the mid-Holocene “thermal maximum” and gradual cooling to pre-industrial global temperature found in the data. Simulated monsoonal precipitation in North Africa peaks between 12 and 9 ka at values ~ 50 % greater than those of the PI, and Indian monsoonal precipitation peaks at 12 and 9 ka at values ~ 45 % greater than the PI. GENMOM captures the reconstructed LGM extent of NH and Southern Hemisphere (SH) sea ice. The simulated present-day Antarctica Circumpolar Current (ACC) is ~ 48 % weaker than observed (62 vs. 119 Sv). The simulated present-day Atlantic Meridional Overturning Circulation (AMOC) of 19.3 ± 1.4 Sv on the Bermuda Rise (33° N) is comparable with the observed value of 17.4 Sv. AMOC at 33° N is reduced by ~ 15 % during the LGM, and the largest post-glacial increase (~ 11 %) occurs, unforced, during the 15 ka time slice.

1 Introduction

The history of the climate system over the past 21 000 years reflects the combined changes in earth-sun orbital geometry, atmospheric greenhouse gas concentrations

CPD

10, 2925–2978, 2014

Global climate simulations at 3000 year intervals

J. R. Alder and
S. W. Hostetler

Title Page

Abstract

Introduction

Conclusions

References

Tables

Figures



Back

Close

Full Screen / Esc

Printer-friendly Version

Interactive Discussion



Global climate simulations at 3000 year intervals

J. R. Alder and
S. W. Hostetler

Title Page

Abstract

Introduction

Conclusions

References

Tables

Figures



Back

Close

Full Screen / Esc

Printer-friendly Version

Interactive Discussion



(GHG), the extent of the Northern Hemisphere (NH) ice sheets, and sea level. GHG levels were lowest during the Last Glacial Maximum (LGM, ~ 21 000 years ago, 21 ka) and increased thereafter to pre-industrial (PI) levels (Brook et al., 2000; Monnin et al., 2001; Sowers et al., 2003). The LGM is further characterized by the large Laurentide (LIS), Cordilleran (CIS) and Fennoscandian (FIS) ice sheets. The height and extent of the ice sheets altered atmospheric circulation patterns, and the extent increased the NH albedo thereby altering the global radiative balance. The effect of the ice sheets on climate progressively diminished from the LGM to early Holocene as global warming driven by increasing GHGs and NH summer insolation accelerated their ablation. Abrupt departures from the comparatively smooth transition from the LGM through the Holocene, such as Heinrich and Dansgaard-Oeschger events, the Bølling–Allerød (BA), and the Younger Dryas (YD), are evident in geologic records, and these events likely influenced the overall trajectory of the deglaciation.

The climate of the past 21 000 years has been studied extensively, beginning with three international collaborative projects: the Long range Investigation, Mapping, and Prediction (CLIMAP; CLIMAP Project Members, 1981) and the Cooperative Holocene Mapping Project (COHMAP; COHMAP Members, 1988), which evolved into the Testing Earth System Models with Paleoenvironmental Observations (TEMPO) project (Kutzbach et al., 1996a, 1998). CLIMAP focused on reconstructing the LGM climate, COHMAP focused on reconstructing the climate of seven time periods (18, 15, 12, 9, 6, 3 ka), and TEMPO focused on reconstructing the climate of 21, 16, 14, 11 and 6 ka. These three projects pioneered data-model comparison through integrating climate model simulations and paleoclimatic data, which motivated the development of new techniques for analyzing geologic data and led to improvements in general circulation models.

More recently, the Palaeoclimate Modelling Intercomparison Project (PMIP) is actively working to advance reconstruction of LGM and 6 ka climate through model-to-model evaluations and data-model comparisons. PMIP has now entered the third phase (PMIP3; Braconnot et al., 2012) and is a component of phase 5 of the Climate

Global climate simulations at 3000 year intervalsJ. R. Alder and
S. W. Hostetler

Title Page

Abstract

Introduction

Conclusions

References

Tables

Figures



Back

Close

Full Screen / Esc

Printer-friendly Version

Interactive Discussion



Model Intercomparison Project (CMIP5). In contrast to CLIMAP, COHMAP, TEMPO and earlier PMIP model experiments that employed fixed sea surface temperatures (SST) and mixed-layer ocean models, some of the PMIP2 experiments and all of the PMIP3 experiments include fully coupled ocean and atmospheric models. In addition, continuous simulations of climate over the last 21 ka have been achieved with earth system models of intermediate complexity (e.g., Timm and Timmermann, 2007), and the TraCE-21ka project at the National Center for Atmospheric Research (NCAR) conducted continuous, transient climate simulations from 22 ka to 6.5 ka with the coupled NCAR Community Climate System Model (Liu et al., 2009). Singarayer and Valdes (2010) simulated the climate of the last 120 000 years using model snapshots at 4 ka and 1 ka intervals.

Here we explore past changes in late-Pleistocene climate using the coupled Atmosphere–Ocean General Circulation Model (AOGCM) GENMOM. We simulated multi-century “time segments” that span the interval from LGM to pre-industrial (PI) every three thousand years (21, 18, 15, 12, 9, 6, 3 ka and PI). The simulations were run with prescribed and time-appropriate insolation, GHG concentrations, continental ice sheets, land extent and sea level as boundary conditions. We analyze the within and between climatology of the time segments and compare the 21 ka and 6 ka results with terrestrial and marine climate reconstructions and results from the PMIP2 and PMIP3 simulations. Braconnot et al. (2012) review some of the highlights of the PMIP2 experiments and the design of the PMIP3 experiments and data and Harrison et al. (2013) evaluate the PMIP3 and PMIP2 simulations of LGM and 6 ka climates with data-model comparisons.

2 Methods

2.1 Model description

GENMOM combines version 3 of the GENESIS atmospheric model (Pollard and Thompson, 1997; Thompson and Pollard, 1995, 1997) with version 2 of the Modular Ocean Model (MOM2, Pacanowski, 1996). Version 3 of GENESIS (Alder et al., 2011; Kump and Pollard, 2008; Pollard and Thompson, 1997; Zhou et al., 2008) incorporates the NCAR CCM3 radiation code (Kiehl et al., 1998). GENESIS has been developed with an emphasis on representing terrestrial physical and biophysical processes, and for application to paleoclimate experiments. Earlier versions of GENESIS (Pollard and Thompson, 1994, 1995, 1997; Thompson and Pollard, 1995, 1997) have been applied in a wide range of modern and paleoclimate studies (Beckmann et al., 2005; Bice et al., 2006; DeConto et al., 2007, 2008; Horton et al., 2007; Hostetler et al., 2006; Miller et al., 2005; Poulsen et al., 2007a, b; Ruddiman et al., 2005; Tabor et al., 2014), and GENESIS simulations with fixed and slab ocean SSTs were included in PMIP1 (Joussaume et al., 1999; Pinot et al., 1999; Pollard et al., 1998).

In our simulations, we employ a coupled model with T31 spectral truncation, which corresponds to a grid of 96 longitudes (3.75°) by 48 Gaussian latitudes ($\sim 3.71^\circ$). The atmosphere is represented by 18 vertical sigma levels with mid-layers ranging from 0.993 at the surface to 0.005 at the tropopause. GENESIS includes the Land Surface eXchange model, LSX, (Pollard and Thompson, 1995) to simulate surface processes and to account for the exchange of energy, mass and momentum between the land surface and the atmospheric boundary layer. MOM2 has 20 fixed-depth vertical levels and is implemented on essentially the same T31 horizontal grid as GENESIS through cosine-weighted distortion (Pacanowski, 1996). Sea ice is simulated by a three-layer model that accounts for local melting, freezing, and fractional cover (Harvey, 1988; Semtner, 1976) and includes the dynamics associated with wind and ocean current using the cavitating-fluid model of Flato and Hibler (1992). The atmospheric and ocean models interact every six hours without flux corrections.

Global climate simulations at 3000 year intervals

J. R. Alder and
S. W. Hostetler

[Title Page](#)[Abstract](#)[Introduction](#)[Conclusions](#)[References](#)[Tables](#)[Figures](#)[Back](#)[Close](#)[Full Screen / Esc](#)[Printer-friendly Version](#)[Interactive Discussion](#)

is constrained and therefore enhanced along and to the south of the southern margin of the LIS extending over the North Atlantic. At 18 ka, a trend toward positive JJA anomalies in 500 hPa heights emerges over the regions of the semi-permanent subtropical high pressure of the North Pacific and central Atlantic. The regions of positive height anomalies, and their associated anticyclonic wind anomalies, expand over central North America, peak from 12 ka through 9 ka, and diminish by 6 ka (Fig. 3). The DJF pattern of low-to-high height anomalies over the North Atlantic is replaced during JJA by a strengthened subtropical high. Anticyclonic flow around positive height anomalies on the western edge of the FIS alters regional flow patterns over and south of the ice sheet. The GENMOM responses to the NH ice sheets are similar to many previous modeling experiments that have established that changes in tropospheric pressure–surface heights and winds are primarily driven by changes in ice-sheet height, and secondarily by temperature and albedo feedbacks (COHMAP Members, 1988; Felzer et al., 1996, 1998; Otto-Bliesner et al., 2006a; Pausata et al., 2011; Pollard and Thompson, 1997; Rind, 1987).

From 21 ka to 12 ka, the largest changes in boreal winter sea-level pressure (SLP) are associated with negative surface temperature anomalies over the continental ice sheets, the landmasses of the NH, and areas of expanded sea ice in the North Atlantic (Fig. 4a) where cooling increases subsidence and thus contributes to cold high surface pressure. Between 21 and 12 ka, changes in the surface-pressure gradient over Africa and the Indian subcontinent reflect a transition in the location and strength of the Hadley circulation as the NH ice sheets melt and global temperature increases, whereas the mid-to-late Holocene changes are the result of changes in the seasonality of insolation and related continental heating and land–sea temperature contrasts. From 21 ka to 15 ka, high pressure over the LIS produces anticyclonic flow across the northern Great Plains and over the Puget Lowlands of the US. Similar anticyclonic tendencies are simulated along the margin of the FIS. Between 12 ka and 6 ka the winter SLP around the Aleutian low in the North Pacific and the Icelandic low in the North Atlantic is strengthened relative to PI.

**Global climate
simulations at 3000
year intervals**J. R. Alder and
S. W. Hostetler[Title Page](#)[Abstract](#)[Introduction](#)[Conclusions](#)[References](#)[Tables](#)[Figures](#)[Back](#)[Close](#)[Full Screen / Esc](#)[Printer-friendly Version](#)[Interactive Discussion](#)

From 21 ka to 9 ka, the JJA SLP anomalies remain strongly positive over the ice sheets and sea ice, whereas from 12 ka to 6 ka the SLP anomalies over Northern Hemisphere landmasses are negative due to lower pressure associated with enhanced continental warming (Fig. 4b). The patterns of the JJA 500 hPa heights, SLP and the associated circulation over North America and adjacent oceans again illustrate similar responses to time-varying controls: changes from 21 ka to 15 ka are primarily driven by changes in the LIS, whereas from 12 ka to 6 ka the circulation changes are related to the changes in the seasonality of Holocene NH insolation (Fig. 2).

3.2 Near-surface air temperature

Our time-segment simulations clearly display surface air temperature (SAT) changes attributed to radiative forcing from the presence of the continental ice sheets, GHGs (Clark et al., 2012), and insolation (Fig. 5). Excluding the BA and YD, the simulations reproduce the rate of warming between 21 ka and 12 ka, but are consistently ~ 0.5 – 0.75 °C colder than the reconstruction of Shakun et al. (2012), likely reflecting cooling over the continental ice sheets that is included in the model average. During the Holocene, between 12 ka and 9 ka our simulations do not reproduce the warming in the Marcott et al. (2013) reconstruction, nor do they capture the gradual cooling trend from the mid-Holocene to PI.

The global average mean annual LGM temperature simulated by GENMOM is 3.8 °C colder than the PI (Table 2, Fig. 5), within the range of cooling in the PMIP2 AOGCM simulations (3.1 to 5.6 and average 4.4 °C) and the PMIP3 simulations (2.6 to 4.9 and average of 4.4 °C) that were forced by similar boundary conditions (Harrison et al., 2013; Kageyama et al., 2006). The LGM cooling is also in agreement with Annan and Hargreaves (2013), who reconciled the PMIP2 ensemble and proxy data to derive an estimated LGM cooling of 4.0 ± 0.8 °C, but falls outside the range of Schmittner et al. (2011b) who found that a median LGM cooling of 3.0 °C (66 % probability range of 2.1 – 3.3 °C). Neither GENMOM nor the ensemble mean of the PMIP3 models capture the ~ 0.5 °C temperature anomaly at 6 ka in the Marcott et al. (2013) reconstruction.

**Global climate
simulations at 3000
year intervals**J. R. Alder and
S. W. Hostetler

Title Page

Abstract

Introduction

Conclusions

References

Tables

Figures



Back

Close

Full Screen / Esc

Printer-friendly Version

Interactive Discussion



The change in the 6 ka global mean annual temperature in the 12 PMIP3 models we analyzed ranged from -0.1 to 0.3 °C with a mean of 0.0 °C. Six models simulated slight warming (average of 0.1 °C) and six simulated slight cooling (average of -0.1 °C).

Seasonal temperature changes across our time-segment simulations illustrate the spatial and temporal effect of changing boundary conditions (Fig. 6). From 21 ka through 15 ka, both DJF and JJA exhibit cold temperature anomalies exceeding 16 °C over and adjacent to the ice sheets in both hemispheres. With the exception of Europe and the high latitudes of the NH, boreal winters remain generally colder than PI over the continents until 3 ka (Fig. 6), corresponding to reduced insolation. NH atmospheric circulation changes induced by atmospheric blocking from the LIS (Fig. 3) sustain warm winter and summer temperature changes over Beringia. Summer warming also occurs south of the FIS. Substantial warming occurs between most pairs of consecutive time segments from the LGM through the Holocene (Fig. 7, Table 2); however, over the African and Indian monsoon regions increased cloudiness associated with enhanced summer monsoonal precipitation leads to cooling from 15 to 6 ka.

The relatively high rate of warming between 18 ka and 15 ka (1.5 °C land and 0.5 °C ocean, Fig. 7, Table 2) is commensurate with increased GHGs (Table 1). Periods of peak annual warming from 15 ka to 12 ka (2.4 °C land and 0.7 °C ocean) and from 12 ka to 9 ka (1.6 °C land and 0.2 °C ocean) are associated with increasing GHG concentrations, ablation of the NH ice sheets (Figs. 1 and 6a), and changes in the seasonality of NH insolation (Fig. 2, Supplement Fig. 4). Although the mid-Holocene wintertime deficit in insolation is small at high northern latitudes, the summertime surface short-wave radiation changes in the model are large and positive (30 – 40 W m⁻²) due to the precessional shift of perihelion, which is reinforced by changes in obliquity. The simulated rates of annual global warming between the LGM and the early Holocene (Fig. 5) are in agreement with data (Clark et al., 2012; Gasse, 2000), and the analyses by Shakun et al. (2012) and Marcott et al. (2013) who attribute a large component of the warming to rising GHG levels.

Global climate simulations at 3000 year intervals

J. R. Alder and
S. W. Hostetler

Title Page

Abstract

Introduction

Conclusions

References

Tables

Figures

◀

▶

◀

▶

Back

Close

Full Screen / Esc

Printer-friendly Version

Interactive Discussion

tion and changing land-SST temperature contrast. The simulated DJF air temperatures in North Africa cool from the LGM until 15 ka, and then warm monotonically through the rest of the deglaciation and Holocene (Fig. 10). Wintertime precipitation over the North African region is minimal. In contrast, JJA temperatures increase throughout the deglaciation, peak at 9 ka, decrease slightly at 6 ka, and increase thereafter. A commensurate increase in JJA precipitation over North Africa between 12 ka and 6 ka is associated with northward migration of the ITCZ (Braconnot et al., 2007a, b; Kutzbach and Liu, 1997), which enhances the transport of moisture into both the North African and Indian monsoon regions. Monsoonal precipitation peaks over both regions between 12 ka and 9 ka (Fig. 10). The change in precipitation between 9 ka and 6 ka over India (0.9 mm d^{-1}) is nearly double the change over North Africa (0.5 mm d^{-1}), consistent with the diagnoses of the mid-Holocene monsoon of Marzin and Braconnot (2009) who attribute the stronger ~ 9 ka monsoon to insolation related to precession and snow cover on the Tibetan Plateau. The pattern of precipitation in the Indian monsoon region is similar to that of North Africa, but exhibits a greater range between peak Holocene values and the PI.

The overall temporal progression and magnitude of precipitation changes in the time-segment simulations are in agreement with the PMIP2 (Braconnot et al., 2007a, b) and PMIP3 simulations at 21 and 6 ka, and with other mid-Holocene modeling studies (Hély et al., 2009; Kutzbach and Liu, 1997; Kutzbach and Otto-Bliesner, 1982; Timm et al., 2010). More specifically, the June through September GENMOM precipitation anomaly of -0.6 mm d^{-1} over the North Africa monsoon region during the LGM is within the range (-0.9 to 0.1 mm d^{-1}) of 5 PMIP2 AOGCMs (Braconnot et al., 2007a) and 7 PMIP3 models (range of -0.6 to 0.2 and average of -0.2 mm d^{-1}). The GENMOM LGM anomaly over India (-0.9 mm d^{-1}) is also within the range (-1.7 to -0.1 mm d^{-1}) of the PMIP2 simulations (Braconnot et al., 2007a) and the PMIP3 simulations (range of -1.3 to 0.0 and average of -0.7 mm d^{-1}).

The northward expansion and spatial pattern of precipitation anomalies of the 6 ka monsoons are in very good agreement with both the PMIP2 and PMIP3 experiments.

Global climate simulations at 3000 year intervals

J. R. Alder and
S. W. Hostetler

Title Page

Abstract

Introduction

Conclusions

References

Tables

Figures



Back

Close

Full Screen / Esc

Printer-friendly Version

Interactive Discussion



Summer precipitation in the GENMOM simulation is enhanced by 0.9 mm d^{-1} relative to PI over North Africa, in agreement with the range (0.2 to 1.4 mm d^{-1}) and mean (0.7 mm d^{-1}) of 11 PMIP2 AOGCMs (Zhao and Harrison, 2012) and 12 PMIP3 models (range of 0.1 to 1.0 and average of 0.6 mm d^{-1}). Over India, the 6 ka GENMOM precipitation anomaly of 1.1 mm d^{-1} exceeds the range (0.2 to 0.9 mm d^{-1}) and mean (0.6 mm d^{-1}) of the 11 PMIP2 models (Zhao and Harrison, 2012), but is within the range of the PMIP3 models (0.5 to 1.3 and average of 1.0 mm d^{-1}).

3.4 Sea ice

DJF sea ice is present in the PI simulation over Hudson Bay, the Arctic Ocean, along the coast of eastern Canada, around Greenland, the Nordic Seas and the Baltic and North Sea (Fig. 11), in agreement with observed present-day distributions (Jaccard et al., 2005). Ice fractions of up to 100 % are simulated over the Bering Sea and the Sea of Okhotsk. In the SH, sea ice persists through austral summer in the Weddell and Ross Seas and a few scattered locations around Antarctica. While the locations of the ice around Antarctica are in agreement with observations (Gersonde et al., 2005), the model underestimates the ice extent over the Weddell Sea and between the Weddell and Ross Seas. The lack of ice is partly attributable to a warm bias in the Southern Ocean associated with the previously mentioned weak ACC (discussed further below). During August and September, simulated sea ice is greatly reduced in the North Atlantic region (Fig. 11), with remnant ice persisting in the extreme north of Baffin Bay and the east coast of Greenland, also in agreement with observations. In the SH, the corresponding winter sea ice grows substantially and the distribution is in generally good agreement with observations (Gersonde et al., 2005).

In both hemispheres, simulated sea-ice fractions display a decreasing trend from the LGM through the early Holocene in response to global warming and obliquity-related changes in insolation (Fig. 11 and Supplement Figs. 13–15). The simulated annual average ice extents for the NH are $9.8 \times 10^6 \text{ km}^2$ for the LGM, $15.8 \times 10^6 \text{ km}^2$ for 6 ka

Global climate simulations at 3000 year intervals

J. R. Alder and
S. W. Hostetler

Title Page

Abstract

Introduction

Conclusions

References

Tables

Figures

◀

▶

◀

▶

Back

Close

Full Screen / Esc

Printer-friendly Version

Interactive Discussion



and $14.1 \times 10^6 \text{ km}^2$ for PI. (Changes in both the distribution and areal coverage of the NH ice reflect the transition of land and ice sheets to ocean in the model surface-type maps as sea level rises.) For the same time periods, the SH ice extents, which are not affected by rising sea level, are $20.9 \times 10^6 \text{ km}^2$, $11.4 \times 10^6 \text{ km}^2$ and $11.1 \times 10^6 \text{ km}^2$, respectively.

During the 21 ka boreal winter, the Arctic Ocean and Baffin Bay are fully covered by ice and the ice around Greenland expands. The model captures the spatial distribution of more sea ice in the western North Atlantic and less ice in the eastern North Atlantic and Nordic Seas where the prescribed FIS margin advances into the water (Fig. 2). The limit of substantial coverage north of 55° N is in agreement with reconstructions (de Vernal et al., 2006) and other LGM simulations (Otto-Bliesner et al., 2006a; Roche et al., 2007); however, slight fractional cover (pack ice) in the model likely extends too far south (to $\sim 45^\circ \text{ N}$) along the coast of North America. Fractional cover of up to 100% is simulated in the far Northwest Pacific and the Sea of Okhotsk with a sharp, southward transition to reduced coverage. In boreal summer of the LGM, simulated sea ice retreats to 65° N in the North Atlantic and persists along eastern Canada, Baffin Bay and south of Greenland and the extreme northern areas of the Nordic Seas.

The overall distribution of SH sea ice (Fig. 11) is in good agreement with reconstructions and other model simulations (Gersonde et al., 2005; Roche et al., 2012). The simulated LGM maximum winter sea ice area is $35.5 \times 10^6 \text{ km}^2$ (72% greater than PI) and the LGM summer minimum is $4.8 \times 10^6 \text{ km}^2$ (112% greater than PI); the winter and summer reconstructed areas are $43.5 \pm 4 \times 10^6 \text{ km}^2$ and $11.1 \pm 4 \times 10^6 \text{ km}^2$, respectively (Roche et al., 2012). The seasonal amplitude (maximum minus minimum) of LGM ice cover simulated by GENMOM ($30.6 \times 10^6 \text{ km}^2$) is comparable with the reconstructed amplitude ($32.4 \pm 4 \times 10^6 \text{ km}^2$) and the LGM-to-PI change of seasonality is well within the range simulated by the PMIP2 models (Roche et al., 2012 their Figs. 2 and 3).

3.5 Antarctic Circumpolar Current and Atlantic Meridional Overturning Circulation

The simulated ACC of 62 Sv is $\sim 48\%$ weaker than the observed value of 119 Sv through the Drake Passage (GECCO data; Köhl and Stammer, 2008). Although the T31 resolution of GENMOM is a factor in limiting flow through the Drake Passage, we attribute the underestimate of the ACC in part to insufficient wind stress at the latitude of the Drake Passage, which is caused by equatorward displacement of the core of the westerly winds, a shortcoming in common with other low-resolution AOGCMs (Alder et al., 2011; Russell et al., 2006; Schmittner et al., 2011a).

Considerable uncertainty exists in the proxies that are used to infer past changes in AMOC strength (Delworth and Zeng, 2008; Lynch-Stieglitz et al., 2007). The $^{231}\text{Pa}/^{230}\text{Th}$ record from 33°N on the Bermuda Rise (Lippold et al., 2009; McManus et al., 2004) indicates that after the LGM the strength of the AMOC began to diminish at $\sim 18\text{ka}$, was further reduced during Heinrich Event 1 (H1) at $\sim 17\text{ka}$, increased abruptly during the BA at 15ka , and weakened again during the YD cold reversal at $\sim 12\text{ka}$. After the YD, the AMOC strengthened again and stabilized. In climate models, a variety of factors including the North Atlantic freshwater budget, model resolution and parameterizations and the characteristics of simulated Antarctic Bottom Water (AABW) give rise to a considerable simulated range of AMOC (Weber et al., 2007).

The AMOC in our PI simulation (Fig. 12) is 19.3 Sv at the core site of 33°N , a value $\sim 2\text{Sv}$ greater than the present-day estimate of 17.4 Sv at 26.5°N (Srokosz et al., 2012). The maximum AMOC simulated by GENMOM in the PI is 21.3 Sv at 41°N , a value outside the range of 13.8 to 20.8 Sv of five models in the PMIP2 experiments (Weber et al., 2007), but within the range of 3.8 to 31.7 Sv of the IPCC AR4 models (Meehl et al., 2007; Schmittner et al., 2005). Analyses of AMOC in the IPCC AR5 and PMIP3 simulations are forthcoming.

Our simulated LGM AMOC at the core site is 16.4 Sv, which is a $\sim 14.7\%$ reduction relative to the PI. The maximum LGM AMOC is 22.4 Sv at 40.8°N , an increase of

Global climate simulations at 3000 year intervals

J. R. Alder and
S. W. Hostetler

Title Page

Abstract

Introduction

Conclusions

References

Tables

Figures



Back

Close

Full Screen / Esc

Printer-friendly Version

Interactive Discussion



**Global climate
simulations at 3000
year intervals**J. R. Alder and
S. W. Hostetler[Title Page](#)[Abstract](#)[Introduction](#)[Conclusions](#)[References](#)[Tables](#)[Figures](#)[Back](#)[Close](#)[Full Screen / Esc](#)[Printer-friendly Version](#)[Interactive Discussion](#)

1.1 Sv (5.1 %) relative to the PI maximum and within the considerable range of -6.2 to $+7.3$ Sv in five PMIP2 simulations (Weber et al., 2007). In the deglacial simulations (21 ka through 15 ka), the northward (positive) AMOC flow extends deeper than that of the PI (Fig. 12) and the southward flow or AABW consequently is somewhat weakened.

The maximum AMOC in GENMOM is essentially constant at 40.8° N depth of 1.23 km for all time segments. Although the depth of the maximum is again comparable to the range of the PMIP2 models (1.24 ± 0.20), the invariance of the location and depth in GENMOM is likely a model-specific response.

Our time-segment simulations display an increase in the strength of AMOC from the LGM to a maximum at 15 ka, decrease to a minimum at 9 ka, and remain more-or-less constant through the PI (Fig. 13), which is in apparent disagreement with the $^{231}\text{Pa}/^{230}\text{Th}$ records from which greater variability is inferred (Lippold et al., 2009; McManus et al., 2004). We do not expect to capture rapid and abrupt climate change events such as H1 (~ 17 ka), the BA (~ 15 ka) and the YD (~ 12 ka) with only eight time segments, because we did not manipulate freshwater discharge to the North Atlantic in our experimental design.

4 21 ka and 6 ka data-model comparisons

We compare temperature and precipitation from our LGM and mid-Holocene simulations with paleoclimatic reconstructions and the PMIP3 simulations. For the LGM, we use the pollen-based reconstructions of mean annual mean temperature (MAT) and precipitation (MAP) from Bartlein et al. (2011) over land, and the Multiproxy Approach for the Reconstruction of the Glacial Ocean Surface Project (MARGO) reconstructions over oceans (Waelbroeck et al., 2009). The gridded $2^\circ \times 2^\circ$ pollen data include > 3000 terrestrial pollen records from Eurasia, Africa and North America, and the global MARGO reconstruction comprises ~ 700 analyses of planktonic foraminifera, diatom, dinoflagellate cyst and radiolarian abundances, alkenones, and planktonic foraminifera Mg/Ca from marine core sites. For 6 ka, we combine the pollen-based reconstructions

data, and the SST anomalies are $\sim 2\text{--}4^\circ\text{C}$ colder over the Western Pacific Warm Pool. Neither GENMOM nor the PMIP3 simulations produce the warming over the central and eastern tropics, or the low latitudes and the North Atlantic that is evident in the MARGO reconstruction.

The simulated LGM MAP anomalies are also comparable with the pollen-based reconstructions (Fig. 14c and d). The model simulates general drying of the NH and a mix of increased and decreased precipitation in Beringia, South America, southern Africa, Southeast (SE) Asia and Australia. GENMOM produces strong drying over and around the NH ice sheets, wetter-than-present conditions in the southwestern United States and drying in Central America. The simulation fails to reproduce the drying over eastern North America that is inferred from the pollen-based data. There is considerable variability in the PMIP3 simulations of MAP (Supplement Figs. 9 and 10). In common with the PMIP3 models, GENMOM simulates a general reduction of precipitation over the NH, the North African and Indian monsoon regions, and SE Asia, and increased precipitation south of the LIS, southern Africa and much of Australia (Supplement Fig. 16).

4.2 6 ka

Relative to PI, the changes in 6 ka boundary conditions are predominantly in the seasonality of insolation (Table 1) as opposed to the stronger radiative forcing associated with changes in GHGs and continental ice sheets from the LGM through the early Holocene. The resulting changes in 6 ka climatology are thus more subtle than those of the deglaciation. The changes of 6 ka MAT simulated by GENMOM are generally within the range of $\pm 1^\circ\text{C}$ (Fig. 15b). Enhanced MAP and associated cooling are evident in the NH monsoonal regions (Fig. 15d). Elsewhere, MAP changes are within a range of $\pm 50\text{ mm}$.

Regionally coherent patterns of temperature anomalies, such as the warming south of Hudson Bay, the contrasting areas of warming over Scandinavia and Western Europe, and cooling in the Mediterranean region, are inferred by the pollen-based data (Fig. 15a). Larger MAT changes at high-elevation sites and regions with anomalies of

CPD

10, 2925–2978, 2014

Global climate simulations at 3000 year intervals

J. R. Alder and
S. W. Hostetler

Title Page

Abstract

Introduction

Conclusions

References

Tables

Figures



Back

Close

Full Screen / Esc

Printer-friendly Version

Interactive Discussion



the PMIP3 models, indicate cooler, drier winters (Supplement Figs. 7 and 11) and regionally variable changes in the summer (Supplement Figs. 8 and 12).

In Africa, the model captures the increase in precipitation in the northern and continental regions and drying along the southern coastal regions, as evident in the data.

5 Strengthening of the African and Indian summer monsoons during the mid-Holocene corresponds well with the PMIP2 and PMIP3 models (Zheng and Braconnot, 2013). Both GENMOM and the data indicate drying over central Scandinavia, wetter conditions over east central Europe, the Iberian Peninsula and around the Mediterranean but, over Western Europe, the simulated decrease in MAP in GENMOM clearly dis-
10 agrees with the data and some of the PMIP3 models (Fig. 15, Supplement Figs. 7, 8 and 16); although, the magnitude of the change in the models is very small and the sign of the change varies among models. Wetter conditions also prevail in Indonesia, and a southwest-to-northeast wet-dry gradient is simulated over Australia.

5 Summary

15 We have presented a suite of multi-century equilibrium climate simulations with GENMOM for the past 21 000 years at 3000 yr intervals. Each 1100 yr simulation was forced with fixed, time-appropriate global boundary conditions that included insolation, GHGs, continental ice sheets and adjustment for sea level. The key drivers of climate change from the LGM through the Holocene are retreat of the NH ice sheets, deglacial increased of GHG concentrations, and latitudinal and seasonal variations in insolation.
20

GENMOM reproduces reasonably well the LGM to Holocene temperature trends inferred from the paleoclimate data syntheses of Shakun et al. (2012) and Marcott et al. (2013). The global LGM cooling of 3.8 °C simulated by GENMOM is within the range of 2.6 to 4.9 °C simulated by the PMIP3 models. Simulated LGM cooling of the
25 tropical oceans is 1.6 °C, which is in good agreement with the MARGO reconstruction of 1.7 ± 1 °C. The magnitude of the global LGM cooling is attributed to the sensitivity of GENMOM to CO₂ (2.2 °C for a 2X increase in the present-day value).

Global climate simulations at 3000 year intervals

J. R. Alder and
S. W. Hostetler

Title Page

Abstract

Introduction

Conclusions

References

Tables

Figures



Back

Close

Full Screen / Esc

Printer-friendly Version

Interactive Discussion



Global climate simulations at 3000 year intervalsJ. R. Alder and
S. W. Hostetler[Title Page](#)[Abstract](#)[Introduction](#)[Conclusions](#)[References](#)[Tables](#)[Figures](#)[Back](#)[Close](#)[Full Screen / Esc](#)[Printer-friendly Version](#)[Interactive Discussion](#)

- Braconnot, P., Harrison, S. P., Kageyama, M., Bartlein, P. J., Masson-Delmotte, V., Abe-Ouchi, A., Otto-Bliesner, B. L., and Zhao, Y.: Evaluation of climate models using palaeoclimatic data, *Nat. Geosci.*, 2, 417–424, doi:10.1038/nclimate1456, 2012.
- Broccoli, A. J., Dahl, K. A., and Stouffer, R. J.: Response of the ITCZ to Northern Hemisphere cooling, *Geophys. Res. Lett.*, 33, L01702, doi:10.1029/2005GL024546, 2006.
- Brohan, P., Kennedy, J. J., Harris, I., Tett, S. F. B., and Jones, P. D.: Uncertainty estimates in regional and global observed temperature changes: a new data set from 1850, *J. Geophys. Res.*, 111, D12106, doi:10.1029/2005JD006548, 2006.
- Brook, E. J., Harder, S., Severinghaus, J., Steig, E. J., and Sucher, C. M.: On the origin and timing of rapid changes in atmospheric methane during the last glacial period, *Global Biogeochem. Cy.*, 14, 559–572, 2000.
- Cheng, H., Sinha, A., Wang, X., Cruz, F. W., and Edwards, R. L.: The Global Paleomonsoon as seen through speleothem records from Asia and the Americas, *Clim. Dynam.*, 39, 1045–1062, doi:10.1007/s00382-012-1363-7, 2012.
- Chiang, J. C. H.: The Tropics in Paleoclimate, *Annu. Rev. Earth Pl. Sc.*, 37, 263–297, doi:10.1146/annurev.earth.031208.100217, 2009.
- Chiang, J. C. H. and Bitz, C. M.: Influence of high latitude ice cover on the marine Intertropical Convergence Zone, *Clim. Dynam.*, 25, 477–496, doi:10.1007/s00382-005-0040-5, 2005.
- Clark, P. U., Shakun, J. D., Baker, P. A., Bartlein, P. J., Brewer, S., Brook, E., Carlson, A. E., Cheng, H., Kaufman, D. S., Liu, Z. Y., Marchitto, T. M., Mix, A. C., Morrill, C., Otto-Bliesner, B. L., Pahnke, K., Russell, J. M., Whitlock, C., Adkins, J. F., Blois, J. L., Clark, J., Colman, S. M., Curry, W. B., Flower, B. P., He, F., Johnson, T. C., Lynch-Stieglitz, J., Markgraf, V., McManus, J., Mitrovica, J. X., Moreno, P. I., and Williams, J. W.: Global climate evolution during the last deglaciation, *P. Natl. Acad. Sci. USA*, 109, E1134–E1142, doi:10.1073/Pnas.1116619109, 2012.
- Claussen, M.: Late Quaternary vegetation-climate feedbacks, *Clim. Past*, 5, 203–216, doi:10.5194/cp-5-203-2009, 2009.
- CLIMAP Project Members: Seasonal reconstructions of the earth's surface at the Last Glacial Maximum, Geological Society of America, Map and Chart Series, MC-36, 1981.
- COHMAP Members: Climatic changes of the last 18 000 years – observations and model simulations, *Science*, 241, 1043–1052, 1988.
- de Vernal, A., Rosell-Mele, A., Kucera, M., Hillaire-Marcel, C., Eynaud, F., Weinelt, M., Dokken, T., and Kageyama, M.: Comparing proxies for the reconstruction of LGM sea-

Global climate simulations at 3000 year intervals

J. R. Alder and
S. W. Hostetler

Title Page

Abstract

Introduction

Conclusions

References

Tables

Figures



Back

Close

Full Screen / Esc

Printer-friendly Version

Interactive Discussion

surface conditions in the northern North Atlantic, *Quaternary Sci. Rev.*, 25, 2820–2834, doi:10.1016/j.quascirev.2006.06.006, 2006.

DeConto, R. M., Pollard, D., and Harwood, D.: Sea ice feedback and Cenozoic evolution of Antarctic climate and ice sheets, *Paleoceanography*, 22, PA3214, doi:10.1029/2006PA001350, 2007.

DeConto, R. M., Pollard, D., Wilson, P. A., Palike, H., Lear, C. H., and Pagani, M.: Thresholds for Cenozoic bipolar glaciation, *Nat. Geosci.*, 455, 652–656, doi:10.1038/nature07337, 2008.

Delworth, T. L. and Zeng, F.: Simulated impact of altered Southern Hemisphere winds on the Atlantic meridional overturning circulation, *Geophys. Res. Lett.*, 35, L20708, doi:10.1029/2008gl035166, 2008.

DiNezio, P. N. and Tierney, J. E.: The effect of sea level on glacial Indo-Pacific climate, *Nat. Geosci.*, 6, 1–7, doi:10.1038/ngeo1823, 2013.

Dorman, J. L. and Sellers, P. J.: A global climatology of albedo, roughness length and stomatal-resistance for atmospheric general-circulation models as represented by the simple biosphere model (Sib), *J. Appl. Meteorol.*, 28, 833–855, doi:10.1175/1520-0450(1989)028<0833:Agcoar>2.0.Co;2, 1989.

Dyke, A. S. and Prest, V. K.: Late Wisconsinan and Holocene History of the Laurentide Ice Sheet, *Géographie physique et Quaternaire*, 1987.

Felzer, B.: Climate impacts of an ice sheet in East Siberia during the Last Glacial Maximum, *Quaternary Sci. Rev.*, 20, 437–447, doi:10.1016/S0277-3791(00)00106-2, 2001.

Felzer, B., Oglesby, R. J., Webb, T., and Hyman, D. E.: Sensitivity of a general circulation model to changes in Northern Hemisphere ice sheets, *J.-Geophys.-Res.*, 101, 19077–19092, 1996.

Felzer, B., Webb, T., and Oglesby, R. J.: The impact of ice sheets, CO₂, and orbital insolation on late quaternary climates: sensitivity experiments with a general circulation model, *Quaternary Sci. Rev.*, 17, 507–534, doi:10.1016/S0277-3791(98)00010-9, 1998.

Flato, G. M. and Hibler, W. D.: Modeling Pack Ice as a Cavitating Fluid, *J. Phys. Oceanogr.*, 22, 626–651, 1992.

Gasse, F.: Hydrological changes in the African tropics since the Last Glacial Maximum, *Quaternary Sci. Rev.*, 19, 189–211, doi:10.1016/S0277-3791(99)00061-X, 2000.

Gates, W. L. and Nelson, A. B.: A new (revised) tabulation of the Scripps topography on a 1 degree global grid, Part 1: Terrain heights, *Tech. Rep. R-1276-1-ARPA*, 1975.

**Global climate
simulations at 3000
year intervals**J. R. Alder and
S. W. Hostetler[Title Page](#)[Abstract](#)[Introduction](#)[Conclusions](#)[References](#)[Tables](#)[Figures](#)[Back](#)[Close](#)[Full Screen / Esc](#)[Printer-friendly Version](#)[Interactive Discussion](#)

Gent, P. R. and McWilliams, J. C.: Isopycnal mixing in ocean circulation models, *J. Phys. Oceanogr.*, 20, 150–155, doi:10.1175/1520-0485(1990)020<0150:IMIOCM>2.0.CO;2, 1990.

Gersonde, R., Crosta, X., Abelmann, A., and Armand, L.: Sea-surface temperature and sea ice distribution of the Southern Ocean at the EPILOG Last Glacial Maximum – a circum-Antarctic view based on siliceous microfossil records, *Quaternary Sci. Rev.*, 24, 869–896, doi:10.1016/j.quascirev.2004.07.015, 2005.

Harrison, S. P., Bartlein, P. J., Brewer, S., Prentice, I. C., Boyd, M., Hessler, I., Holmgren, K., Izumi, K., and Willis, K.: Climate model benchmarking with glacial and mid-Holocene climates, *Clim. Dynam.*, 1–18, doi:10.1007/s00382-013-1922-6, 2013.

Harvey, L. D. D.: Development of a sea ice model for use in zonally averaged energy balance climate models, *J. Climate*, 1, 1221–1238, 1988.

Hassol, S. J.: Impacts of a Warming Arctic – Arctic Climate Impact Assessment, Arctic Climate Impact Assessment, ISBN 0521617782, Cambridge University Press, Cambridge, UK, 144 pp., 2004.

Hély, C., Braconnot, P., Watrin, J., and Zheng, W.: Climate and vegetation: simulating the African humid period, *CR Geosci.*, 341, 671–688, doi:10.1016/j.crte.2009.07.002, 2009.

Horton, D. E., Poulsen, C. J., and Pollard, D.: Orbital and CO₂ forcing of late Paleozoic continental ice sheets, *Geophys. Res. Lett.*, 34, L19708, doi:10.1029/2007GL031188, 2007.

Hostetler, S. W., Clark, P. U., Bartlein, P. J., Mix, A. C., and Pisias, N. J.: Atmospheric transmission of North Atlantic Heinrich events, *J.-Geophys.-Res.*, 104, 3947–3952, 1999.

Hostetler, S. W., Pisias, N., and Mix, A. C.: Sensitivity of Last Glacial Maximum climate to uncertainties in tropical and subtropical ocean temperatures, *Quaternary Sci. Rev.*, 25, 1168–1185, doi:10.1016/j.quascirev.2005.12.010, 2006.

Jaccard, S. L., Haug, G. H., Sigman, D. M., Pedersen, T. F., Thierstein, H. R., and Rohl, U.: Glacial/interglacial changes in subarctic North Pacific stratification, *Science*, 308, 1003–1006, doi:10.1126/science.1108696, 2005.

Joussaume, S., Taylor, K. E., Braconnot, P., Mitchell, J., Kutzbach, J. E., Harrison, S. P., Prentice, I. C., Broccoli, A. J., Abe-Ouchi, A., Bartlein, P. J., Bonfils, C., Dong, B., Guiot, J., Herterich, K., Hewitt, C. D., Jolly, D., Kim, J. W., Kislov, A., Kitoh, A., Loutre, M. F., Mason, V., McAvaney, B., McFarlane, N., de Noblet, N., Peltier, W. R., Peterschmitt, J. Y., Pollard, D., Rind, D., Royer, J. F., Schlesinger, M. E., Syktus, J., Thompson, S. L., Valdes, P., Vettoretti, G., Webb, R. S., and Wypytta, U.: Monsoon changes for 6000 years ago: results

Global climate simulations at 3000 year intervals

J. R. Alder and
S. W. Hostetler

Title Page

Abstract

Introduction

Conclusions

References

Tables

Figures



Back

Close

Full Screen / Esc

Printer-friendly Version

Interactive Discussion

of 18 simulations from the Paleoclimate Modeling Intercomparison Project (PMIP), *Geophys. Res. Lett.*, 26, 859–862, 1999.

Kageyama, M., D'Andrea, F., Ramstein, G., Valdes, P. J., and Vautard, R.: Weather regimes in past climate atmospheric general circulation model simulations, *Clim. Dynam.*, 15, 773–793, doi:10.1007/S003820050315, 1999.

Kageyama, M., Laîné, A., Abe-Ouchi, A., Braconnot, P., Cortijo, E., Crucifix, M., de Vernal, A., Guiot, J., Hewitt, C. D., and Kitoh, A.: Last Glacial Maximum temperatures over the North Atlantic, Europe and western Siberia: a comparison between PMIP models, MARGO sea-surface temperatures and pollen-based reconstructions, *Quaternary Sci. Rev.*, 25, 2082–2102, doi:10.1016/j.quascirev.2006.02.010, 2006.

Kalnay, E., Kanamitsu, M., Kistler, R., Collins, W., Deaven, D., Gandin, L., Iredell, M., Saha, S., White, G., Woollen, J., Zhu, Y., Chelliah, M., Ebisuzaki, W., Higgins, W., Janowiak, J., Mo, K. C., Ropelewski, C., Wang, J., Leetmaa, A., Reynolds, R., Jenne, R., and Joseph, D.: The NCEP/NCAR 40 year reanalysis project, *B. Am. Meteorol. Soc.*, 77, 437–471, 1996.

Kiehl, J. T., Hack, J. J., Bonan, G. B., Boville, B. A., Williamson, D. L., and Rasch, P. J.: The National Center for Atmospheric Research Community Climate Model: CCM3, *J. Climate*, 11, 1131–1149, 1998.

Kim, S.-J., Crowley, T. J., Erickson, D. J., Govindasamy, B., Duffy, P. B., and Lee, B. Y.: High-resolution climate simulation of the last glacial maximum, *Clim. Dynam.*, 31, 1–16, doi:10.1007/s00382-007-0332-z, 2007.

Köhl, A. and Stammer, D.: Decadal sea level changes in the 50 year GECCO ocean synthesis, *J. Climate*, 21, 1876–1890, doi:10.1175/2007JCLI2081.1, 2008.

Kump, L. R. and Pollard, D.: Amplification of cretaceous warmth by biological cloud feedbacks, *Science*, 320, 195–195, doi:10.1126/science.1153883, 2008.

Kutzbach, J. E. and Liu, Z.: Response of the African Monsoon to orbital forcing and ocean feedbacks in the middle holocene, *Science*, 278, 440–443, doi:10.1126/science.278.5337.440, 1997.

Kutzbach, J. E. and Otto-Bliesner, B. L.: The sensitivity of the African–Asian monsoonal climate to orbital parameter changes for 9000 years BP in a low-resolution general-circulation model, *J. Atmos. Sci.*, 39, 1177–1188, 1982.

Kutzbach, J. E., Bartlein, P. J., FOLEY, J. A., Harrison, S. P., Hostetler, S. W., Liu, Z., Prentice, I. C., and WEBB, T. I.: Potential role of vegetation feedback in the climate sensitivity of

Global climate simulations at 3000 year intervals

J. R. Alder and
S. W. Hostetler

Title Page

Abstract

Introduction

Conclusions

References

Tables

Figures



Back

Close

Full Screen / Esc

Printer-friendly Version

Interactive Discussion

high-latitude regions: a case study at 6000 years B.P, *Global Biogeochem. Cy.*, 10, 727–736, 1996a.

Kutzbach, J., Bonan, G., Foley, J., and Harrison, S. P.: Vegetation and soil feedbacks on the response of the African monsoon to orbital forcing in the early to middle Holocene, *Nature*, 384, 623–626, doi:10.1038/384623a0, 1996b.

Kutzbach, J., Gallimore, R., Harrison, S., Behling, P., Selin, R., and Laarif, F.: Climate and biome simulations for the past 21 000 years, *Quaternary Sci. Rev.*, 17, 473–506, 1998.

Leduc, G., Schneider, R., Kim, J. H., and Lohmann, G.: Holocene and Eemian sea surface temperature trends as revealed by alkenone and Mg/Ca paleothermometry, *Quaternary Sci. Rev.*, 29, 989–1004, doi:10.1016/j.quascirev.2010.01.004, 2010.

Lee, J.-Y., and Wang, B.: Future change of global monsoon in the CMIP5, *Clim. Dynam.*, 42, 101–119, doi:10.1007/s00382-012-1564-0, 2014.

Li, C. and Battisti, D. S.: Reduced Atlantic storminess during Last Glacial Maximum: evidence from a coupled climate model, *J. Climate*, 21, 3561–3579, doi:10.1175/2007jcli2166.1, 2008.

Licciardi, J. M., Clark, P. U., Jenson, J. W., and Macayeal, D. R.: Deglaciation of a soft-bedded Laurentide ice sheet, *Quaternary Sci. Rev.*, 17, 427–448, doi:10.1016/S0277-3791(97)00044-9, 1998.

Lippold, J., Grützner, J., Winter, D., Lahaye, Y., Mangini, A., and Christl, M.: Does sedimentary $^{231}\text{Pa}/^{230}\text{Th}$ from the Bermuda rise monitor past Atlantic meridional overturning circulation? *Geophys. Res. Lett.*, 36, L12601, doi:10.1029/2009gl038068, 2009.

Liu, Z., Otto-Bliesner, B. L., He, F., Brady, E. C., Tomas, R., Clark, P. U., Carlson, A. E., Lynch-Stieglitz, J., Curry, W., Brook, E., Erickson, D., Jacob, R., Kutzbach, J., and Cheng, J.: Transient simulation of last deglaciation with a new mechanism for Bolling–Allerod warming, *Science*, 325, 310–314, doi:10.1126/science.1171041, 2009.

Lynch-Stieglitz, J., Adkins, J. F., Curry, W. B., Dokken, T., Hall, I. R., Herguera, J. C., Hirschi, J. J., Ivanova, E. V., Kissel, C., Marchal, O., Marchitto, T. M., McCave, I. N., McManus, J. F., Mulitza, S., Ninnemann, U., Peeters, F., Yu, E. F., and Zahn, R.: Atlantic meridional overturning circulation during the Last Glacial Maximum, *Science*, 316, 66–69, doi:10.1126/science.1137127, 2007.

Marcott, S. A., Shakun, J. D., Clark, P. U., and Mix, A. C.: A reconstruction of regional and global temperature for the past 11 300 years, *Science*, 339, 1198–1201, doi:10.1126/Science.1228026, 2013.

**Global climate
simulations at 3000
year intervals**J. R. Alder and
S. W. Hostetler[Title Page](#)[Abstract](#)[Introduction](#)[Conclusions](#)[References](#)[Tables](#)[Figures](#)[Back](#)[Close](#)[Full Screen / Esc](#)[Printer-friendly Version](#)[Interactive Discussion](#)

Marzin, C. and Braconnot, P.: Variations of Indian and African monsoons induced by insolation changes at 6 and 9.5 kyr BP, *Clim. Dynam.*, 33, 215–231, doi:10.1007/s00382-009-0538-3, 2009.

McManus, J. F., Francois, R., Gherardi, J. M., Keigwin, L. D., and Brown-Leger, S.: Collapse and rapid resumption of Atlantic meridional circulation linked to deglacial climate changes, *Nature*, 428, 834–837, doi:10.1038/Nature02494, 2004.

Meehl, G. A., Stocker, T. F., and Collins, W. D.: Global climate projections, in: *Climate Change 2007: The Physical Science Basis. Contribution of Working Group I to the Fourth Assessment Report of the Intergovernmental Panel on Climate Change*, edited by: Solomon, S., Qin, D., Manning, M., Chen, Z., Marquis, M., Averyt, K. B., Tignor, M., and Miller, H. L., Cambridge University Press, Cambridge, UK and New York, NY, USA, 2007.

Miller, G., Mangan, J., Pollard, D., Thompson, S. L., Felzer, B., and Magee, J.: Sensitivity of the Australian Monsoon to insolation and vegetation: implications for human impact on continental moisture balance, *Geology*, 33, 65–68, 2005.

Moller, T., Schulz, H., and Kucera, M.: The effect of sea surface properties on shell morphology and size of the planktonic foraminifer *Neogloboquadrina pachyderma* in the North Atlantic, *Palaeogeogr. Palaeoclimatol.*, 391, 34–48, doi:10.1016/j.palaeo.2011.08.014, 2013.

Monnin, E., Indermuhle, A., Dallenbach, A., Fluckiger, J., Stauffer, B., Stocker, T. F., Raynaud, D., and Barnola, J. M.: Atmospheric CO₂ concentrations over the last glacial termination, *Science*, 291, 112–114, 2001.

Otto-Bliesner, B. L., Brady, E. C., Clauzet, G., Tomas, R., Levis, S., and Kothavala, Z.: Last Glacial Maximum and Holocene climate in CCSM3, *J. Climate*, 19, 2526–2544, doi:10.1175/Jcli3748.1, 2006a.

Otto-Bliesner, B. L., Tomas, R., Brady, E. C., Ammann, C., Kothavala, Z., and Clauzet, G.: Climate sensitivity of moderate- and low-resolution versions of CCSM3 to preindustrial forcings, *J. Climate*, 19, 2567–2583, doi:10.1175/Jcli3754.1, 2006b.

Otto-Bliesner, B. L., Schneider, R., Brady, E. C., Kucera, M., Abe-Ouchi, A., Bard, E., Braconnot, P., Crucifix, M., Hewitt, C. D., Kageyama, M., Marti, O., Paul, A., Rosell-Mele, A., Waelbroeck, C., Weber, S. L., Weinelt, M., and Yu, Y.: A comparison of PMIP2 model simulations and the MARGO proxy reconstruction for tropical sea surface temperatures at last glacial maximum, *Clim. Dynam.*, 32, 799–815, doi:10.1007/s00382-008-0509-0, 2009.

Pacanowski, R. C.: MOM 2 Version 2.0 (Beta) Documentation: User's Guide and Reference Manual, NOAA GFDL Ocean Technical Report 3.2. 1996.

Global climate simulations at 3000 year intervals

J. R. Alder and
S. W. Hostetler

Title Page

Abstract

Introduction

Conclusions

References

Tables

Figures



Back

Close

Full Screen / Esc

Printer-friendly Version

Interactive Discussion



Pausata, F. S. R., Li, C., Wettstein, J. J., Kageyama, M., and Nisancioglu, K. H.: The key role of topography in altering North Atlantic atmospheric circulation during the last glacial period, *Clim. Past*, 7, 1089–1101, doi:10.5194/cp-7-1089-2011, 2011.

Peixoto, J. P. and Oort, A. H.: *The Physics of Climate*, 3rd ed., American Institute of Physics, 1992.

Peltier, W. R.: Global glacial isostatic adjustment: palaeogeodetic and space-geodetic tests of the ICE-4G (VM2) model, *J. Quaternary Sci.*, 17, 491–510, doi:10.1002/jqs.713, 2002.

Pinot, S., Ramstein, G., Harrison, S. P., Prentice, I. C., Guiot, J., Stute, M., and Joussaume, S.: Tropical paleoclimates at the Last Glacial Maximum: comparison of Paleoclimate Modelling Intercomparison Project (PMIP) simulations and paleodata, *Clim. Dynam.*, 15, 857–874, 1999.

Pollard, D. and Reusch, D. B.: A calendar conversion method for monthly mean paleoclimate model output with orbital forcing, *J.-Geophys.-Res.*, 107, 4615, doi:10.1029/2002JD002126, 2002.

Pollard, D. and Thompson, S. L.: Sea-ice dynamics and CO₂ sensitivity in a global climate model, *Atmos.-Ocean*, 32, 449–467, doi:10.1080/07055900.1994.9649506, 1994.

Pollard, D. and Thompson, S. L.: Use of a Land-Surface-Transfer Scheme (Lsx) in a global climate model – the response to doubling stomatal-resistance, *Glob. Planet. Change*, 10, 129–161, doi:10.1016/0921-8181(94)00023-7, 1995.

Pollard, D. and Thompson, S. L.: Climate and ice-sheet mass balance at the last glacial maximum from the genesis version 2 global climate model, *Quaternary Sci. Rev.*, 16, 841–863, 1997.

Pollard, D., Bergengren, J. C., Stillwell-Soller, L. M., Felzer, B., and Thompson, S. L.: Climate simulations for 10 000 and 6000 years BP using the GENESIS global climate model, *Palaeoclimates: Data and Modelling, Palaeoclimates – Data and Modelling*, 1998.

Poulsen, C. J., Pollard, D., and White, T. S.: General circulation model simulation of the delta O-18 content of continental precipitation in the middle Cretaceous: a model-proxy comparison, *Geology*, 35, 199–202, doi:10.1130/G23343A.1, 2007a.

Poulsen, C. J., Pollard, D., Montanez, I. P., and Rowley, D.: Late Paleozoic tropical climate response to Gondwanan deglaciation, *Geology*, 35, 771–774, doi:10.1130/G23841A.1, 2007b.

Ramstein, G. and Joussaume, S.: Sensitivity experiments to sea surface temperatures, sea-ice extent and ice-sheet reconstruction for the Last Glacial Maximum, *Ann. Glaciol.*, 21, 343–347, 1995.

Global climate simulations at 3000 year intervalsJ. R. Alder and
S. W. Hostetler[Title Page](#)[Abstract](#)[Introduction](#)[Conclusions](#)[References](#)[Tables](#)[Figures](#)[Back](#)[Close](#)[Full Screen / Esc](#)[Printer-friendly Version](#)[Interactive Discussion](#)

- Srokosz, M., Baringer, M., Bryden, H., Cunningham, S., Delworth, T., Lozier, S., Marotzke, J., and Sutton, R.: Past, present, and future changes in the atlantic meridional overturning circulation, *B. Am. Meteorol. Soc.*, 93, 1663–1676, doi:10.1175/bams-d-11-00151.1, 2012.
- Tabor, C. R., Poulsen, C. J., and Pollard, D.: Mending Milankovitch's theory: obliquity amplification by surface feedbacks, *Clim. Past*, 10, 41–50, doi:10.5194/cp-10-41-2014, 2014.
- Thompson, S. L. and Pollard, D.: A global climate model (Genesis) with a Land-Surface Transfer Scheme (LSX) .1. Present climate simulation, *J. Climate*, 8, 732–761, 1995.
- Thompson, S. L. and Pollard, D.: Greenland and Antarctic mass balances for present and doubled atmospheric CO₂ from the GENESIS version-2 global climate model, *J. Climate*, 10, 871–900, 1997.
- Timm, O. and Timmermann, A.: Simulation of the last 21 000 years using accelerated transient boundary conditions, *J. Climate*, 20, 4377–4401, doi:10.1175/JCLI4237.1, 2007.
- Timm, O., Timmermann, A., Abe-Ouchi, A., Saito, F., and Segawa, T.: On the definition of seasons in paleoclimate simulations with orbital forcing, *Paleoceanography*, 23, PA2221, doi:10.1029/2007PA001461, 2008.
- Timm, O., Köhler, P., Timmermann, A., and Menviel, L.: Mechanisms for the onset of the African humid period and Sahara greening 14.5–11 ka BP, *J. Climate*, 23, 2612–2633, doi:10.1175/2010jcli3217.1, 2010.
- Unterman, M. B., Crowley, T. J., Hodges, K. I., Kim, S. J., and Erickson, D. J.: Paleometeorology: high resolution Northern Hemisphere wintertime mid-latitude dynamics during the Last Glacial Maximum, *Geophys. Res. Lett.*, 38, L23702, doi:10.1029/2011gl049599, 2011.
- Waelbroeck, C., Paul, A., Kucera, M., Rosell-Mele, A., Weinelt, M., Schneider, R., Mix, A. C., Abelmann, A., Armand, L., Bard, E., Barker, S., Barrows, T. T., Benway, H., Cacho, I., Chen, M. T., Cortijo, E., Crosta, X., de Vernal, A., Dokken, T., Duprat, J., Elderfield, H., Eynaud, F., Gersonde, R., Hayes, A., Henry, M., Hillaire-Marcel, C., Huang, C. C., Jansen, E., Juggins, S., Kallel, N., Kiefer, T., Kienast, M., Labeyrie, L., Leclaire, H., Londeix, L., Mangin, S., Matthiessen, J., Marret, F., Meland, M., Morey, A. E., Mulitza, S., Pflaumann, U., Pisias, N. G., Radi, T., Rochon, A., Rohling, E. J., Saffi, L., Schaefer-Neth, C., Solignac, S., Spero, H., Tachikawa, K., Turon, J. L., and Members, M. P.: Constraints on the magnitude and patterns of ocean cooling at the Last Glacial Maximum, *Nat. Geosci.*, 2, 127–132, doi:10.1038/NGEO411, 2009.
- Weber, S. L., Driifhout, S. S., Abe-Ouchi, A., Crucifix, M., Eby, M., Ganopolski, A., Murakami, S., Otto-Bliesner, B., and Peltier, W. R.: The modern and glacial overturning circulation in the

Atlantic ocean in PMIP coupled model simulations, *Clim. Past*, 3, 51–64, doi:10.5194/cp-3-51-2007, 2007.

Zhao, Y. and Harrison, S. P.: Mid-Holocene monsoons: a multi-model analysis of the inter-hemispheric differences in the responses to orbital forcing and ocean feedbacks, *Clim. Dynam.*, 39, 1457–1487, doi:10.1007/s00382-011-1193-z, 2012.

Zheng, W. and Braconnot, P.: Characterization of model spread in PMIP2 mid-holocene simulations of the African monsoon, *J. Climate*, 26, 1192–1210, doi:10.1175/JCLI-D-12-00071.1, 2013.

Zhou, J., Poulsen, C. J., Pollard, D., and White, T. S.: Simulation of modern and middle Cretaceous marine delta $\delta^{18}\text{O}$ with an ocean–atmosphere general circulation model, *Paleoceanography*, 23, PA3223, doi:10.1029/2008pa001596, 2008.

CPD

10, 2925–2978, 2014

Global climate simulations at 3000 year intervals

J. R. Alder and
S. W. Hostetler

Title Page

Abstract

Introduction

Conclusions

References

Tables

Figures

◀

▶

◀

▶

Back

Close

Full Screen / Esc

Printer-friendly Version

Interactive Discussion



Global climate simulations at 3000 year intervals

J. R. Alder and
S. W. Hostetler

Title Page

Abstract

Introduction

Conclusions

References

Tables

Figures

◀

▶

◀

▶

Back

Close

Full Screen / Esc

Printer-friendly Version

Interactive Discussion



Table 1. Atmospheric greenhouse gas concentrations for each time-segment simulation. The 21 ka through 3 ka values for CO₂ (Monnin et al., 2001), CH₄ (Brook et al., 2000) and N₂O (Sowers et al., 2003) are estimated from ice core records by averaging the gas concentrations within a ± 300 yr window centered at the time of interest. For comparison, the PMIP3 concentrations for 6 ka are 280 ppmV, 650 ppbV, and 270 ppbV for CO₂, CH₄ and N₂O respectively, and 185 ppmV, 350 ppbV, and 200 ppbV for 21 ka. In the table, e is eccentricity, $\omega - 180$ is precession and ε is obliquity (Berger and Loutre, 1991).

	CO ₂ (ppmV)	CH ₄ (ppbV)	N ₂ O (ppbV)	e	$\omega - 180$	ε
PD	355	1714	311	0.0176	101.37	23.446
PI	280	760	270	0.0176	101.37	23.446
3 ka	275	627	264	0.0183	50.30	23.815
6 ka	260	596	227	0.0192	0.01	24.100
9 ka	260	677	244	0.0198	310.32	24.229
12 ka	240	500	246	0.0201	261.07	24.161
15 ka	220	500	216	0.0202	212.04	23.895
18 ka	188	382	219	0.0199	163.04	23.475
21 ka	188	392	199	0.0194	113.98	22.989

Global climate simulations at 3000 year intervals

J. R. Alder and
S. W. Hostetler

Title Page

Abstract

Introduction

Conclusions

References

Tables

Figures

◀

▶

◀

▶

Back

Close

Full Screen / Esc

Printer-friendly Version

Interactive Discussion



Table 2. Annual average 2 m air temperatures and precipitation rates for the time segment simulations. NCEP is from the National Center for Environmental Prediction NCEP/NCAR Reanalysis data set (Kalnay et al., 1996), PD2X is the $2 \times \text{CO}_2$ simulation, PD is present day and PI is pre-industrial. Parenthetical values are the changes from the previous segment, e.g., the global average temperature for the PD is 0.77°C warmer than the PI.

	Temperature (K)			Precipitation (mm d^{-1})		
	Global	Land	Ocean	Global	Land	Ocean
NCEP (1980–2000)	287.52 –	281.66 –	289.84 –	3.09 –	2.30 –	3.40 –
PD2X	288.48 (2.2)	282.06 (2.69)	291.29 (1.91)	3.11 (0.11)	2.17 (0.10)	3.53 (0.13)
PD	286.34 (0.77)	279.37 (0.93)	289.38 (0.70)	3.00 (0.04)	2.07 (0.04)	3.40 (0.05)
PI	285.57 (0.07)	278.44 (–0.03)	288.68 (0.15)	2.95 (0.00)	2.03 (–0.02)	3.36 (0.02)
3 ka	285.50 (0.32)	278.47 (0.30)	288.53 (0.33)	2.95 (0.02)	2.05 (0.00)	3.34 (0.04)
6 ka	285.17 (0.23)	278.18 (0.95)	288.20 (–0.27)	2.93 (0.02)	2.05 (0.00)	3.30 (0.02)
9 ka	284.95 (0.74)	277.23 (1.63)	288.47 (0.22)	2.91 (0.05)	2.05 (0.06)	3.30 (0.03)
12 ka	284.21 (1.40)	275.60 (2.44)	288.25 (0.70)	2.86 (0.09)	1.99 (0.12)	3.26 (0.05)
15 ka	282.81 (0.93)	273.16 (1.53)	287.55 (0.53)	2.77 (0.05)	1.87 (0.09)	3.21 (0.02)
18 ka	281.88 (0.16)	271.63 (0.28)	287.02 (0.06)	2.72 (0.01)	1.78 (0.01)	3.19 (0.01)
21 ka	281.72	271.35	286.96	2.71	1.78	3.18

Table A1. List of abbreviations and acronyms.

AABW	Antarctic Bottom Water
ACC	Antarctic Circumpolar Current
AMOC	Atlantic Meridional Overturning Circulation
AOGCM	Atmosphere–Ocean General Circulation Model
BA	Bølling–Allerød
CIS	Cordilleran Ice Sheet
CLIMAP	Climate: Long range Investigation, Mapping, and Prediction
COHMAP	Cooperative Holocene Mapping Project
DJF	December, January and February
FIS	Fennoscandian Ice Sheet
GECCO	German partner of Estimating the Circulation and Climate of the Ocean
GENESIS	Global Environmental and Ecological Simulation of Interactive Systems
GHG	Greenhouse gas
ITCZ	Intertropical Convergence Zone
H1	Heinrich Event 1
JJA	June, July and August
LGM	Last Glacial Maximum
LIS	Laurentide Ice Sheet
LSX	Land Surface eXchange
MAM	March, April and May
MAP	Mean annual precipitation
MARGO	Multiproxy Approach for the Reconstruction of the Glacial Ocean Surface Project
MAT	Mean annual temperature
MOM2	Modular Ocean Model version 2
NCAR	National Center for Atmospheric Research
NCEP	National Centers for Environmental Prediction
NH	Northern Hemisphere
OSU-LIS	Oregon State University Laurentide Ice Sheet
PD	Present-day
PI	Pre-industrial
PMIP	Palaeoclimate Modelling Intercomparison Project
SH	Southern Hemisphere
SLP	Sea-level pressure
SON	September, October and November
SST	Sea surface temperature
TEMPO	Testing Earth System Models with Paleoenvironmental Observations
YD	Younger Dryas

Global climate simulations at 3000 year intervals

J. R. Alder and
S. W. Hostetler

[Title Page](#)

[Abstract](#) [Introduction](#)

[Conclusions](#) [References](#)

[Tables](#) [Figures](#)

[◀](#) [▶](#)

[◀](#) [▶](#)

[Back](#) [Close](#)

[Full Screen / Esc](#)

[Printer-friendly Version](#)

[Interactive Discussion](#)



Global climate simulations at 3000 year intervals

J. R. Alder and
S. W. Hostetler

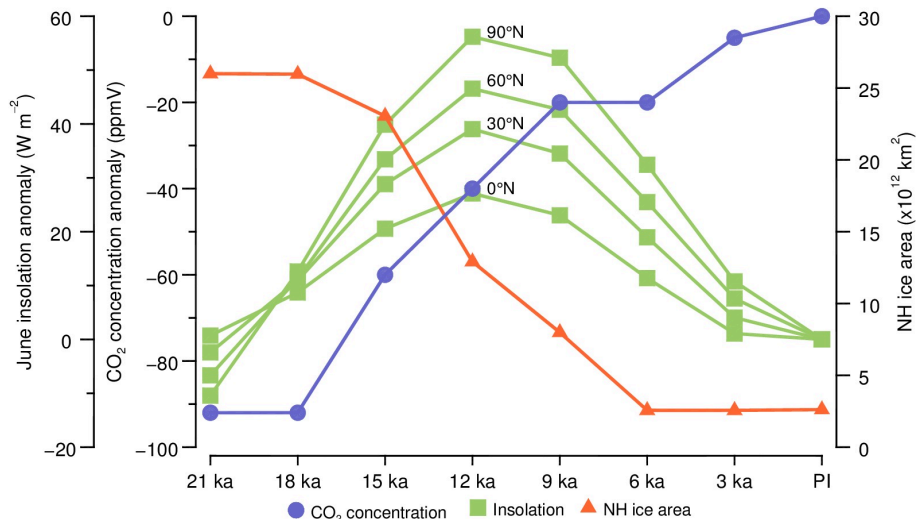


Figure 1. Boundary conditions for the time-segment simulations. CO_2 concentrations are relative to the PI concentration of 280 ppmV. NH ice area is the total area covered by the continental ice sheets. June insolation anomalies are relative to PI at the indicated latitude. Insolation data from Berger and Loutre (1991).

Global climate simulations at 3000 year intervals

J. R. Alder and
S. W. Hostetler

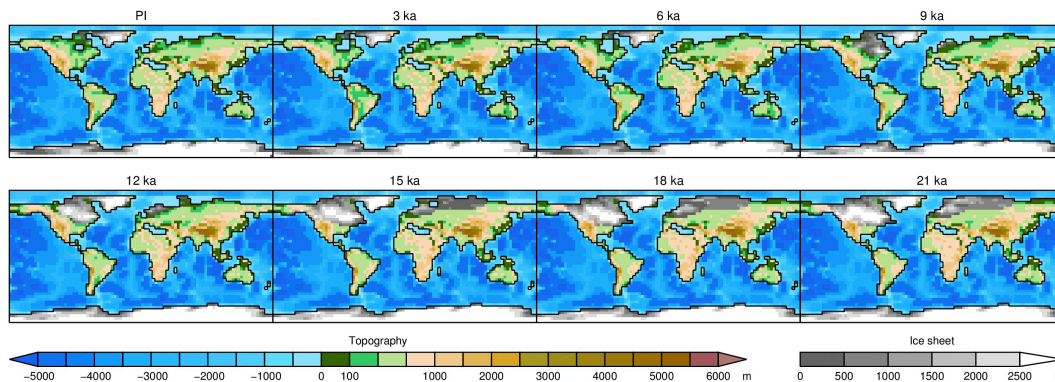


Figure 2. Orography for the time-segment simulations, with ice sheet height and extent derived from ICE-4G (Peltier, 2002) for the Fennoscandian, Cordilleran and Antarctic, and OSU-LIS (Licciardi et al., 1998) for the Laurentide.

[Title Page](#)[Abstract](#)[Introduction](#)[Conclusions](#)[References](#)[Tables](#)[Figures](#)[Back](#)[Close](#)[Full Screen / Esc](#)[Printer-friendly Version](#)[Interactive Discussion](#)

Global climate simulations at 3000 year intervals

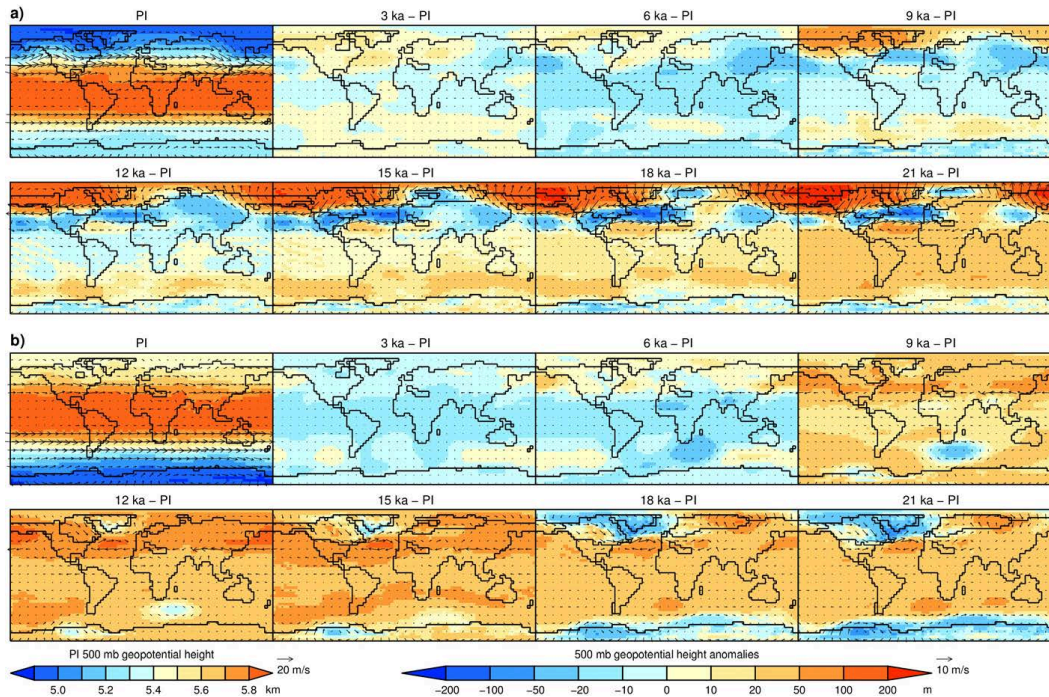
J. R. Alder and
S. W. Hostetler

Figure 3. Simulated seasonal 500 hPa geopotential height and wind anomalies relative to PI. **(a)** December, January, and February and **(b)** June, July and August. Raw 500 hPa geopotential height and wind are shown in Supplement Fig. 2.

Title Page

Abstract

Introduction

Conclusions

References

Tables

Figures

◀

▶

◀

▶

Back

Close

Full Screen / Esc

Printer-friendly Version

Interactive Discussion



Global climate simulations at 3000 year intervals

J. R. Alder and
S. W. Hostetler

[Title Page](#)

[Abstract](#)

[Introduction](#)

[Conclusions](#)

[References](#)

[Tables](#)

[Figures](#)



[Back](#)

[Close](#)

[Full Screen / Esc](#)

[Printer-friendly Version](#)

[Interactive Discussion](#)

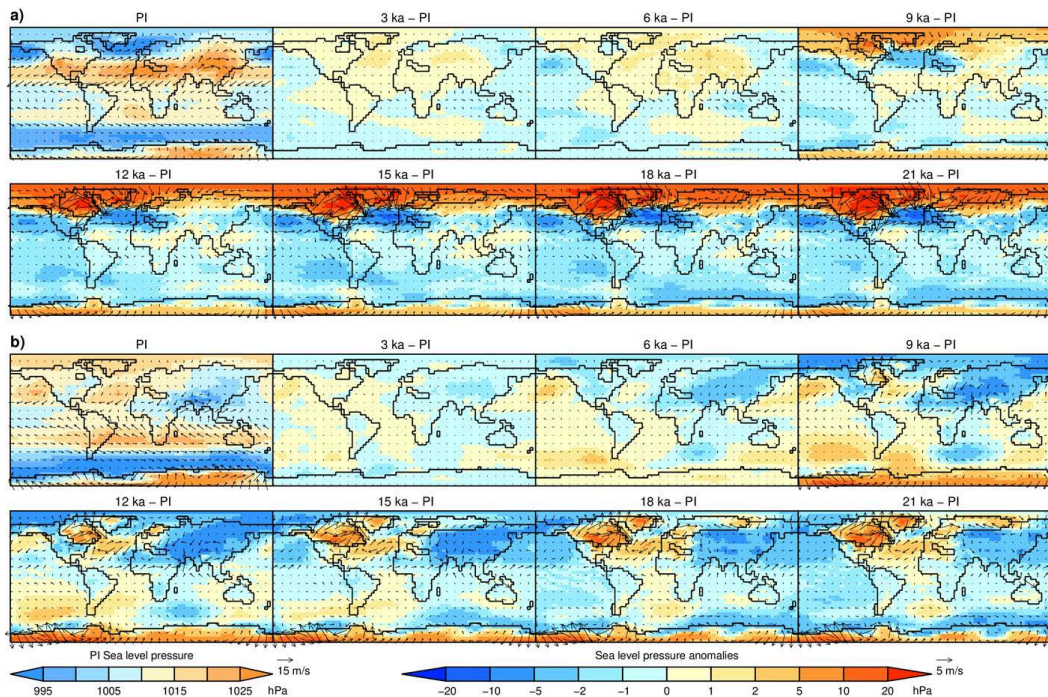


Figure 4. Simulated seasonal average sea-level pressure and 2 m wind anomalies relative to PI. **(a)** December, January, and February and **(b)** June, July, and August. Raw sea level pressure and wind are shown in Supplement Fig. 3.

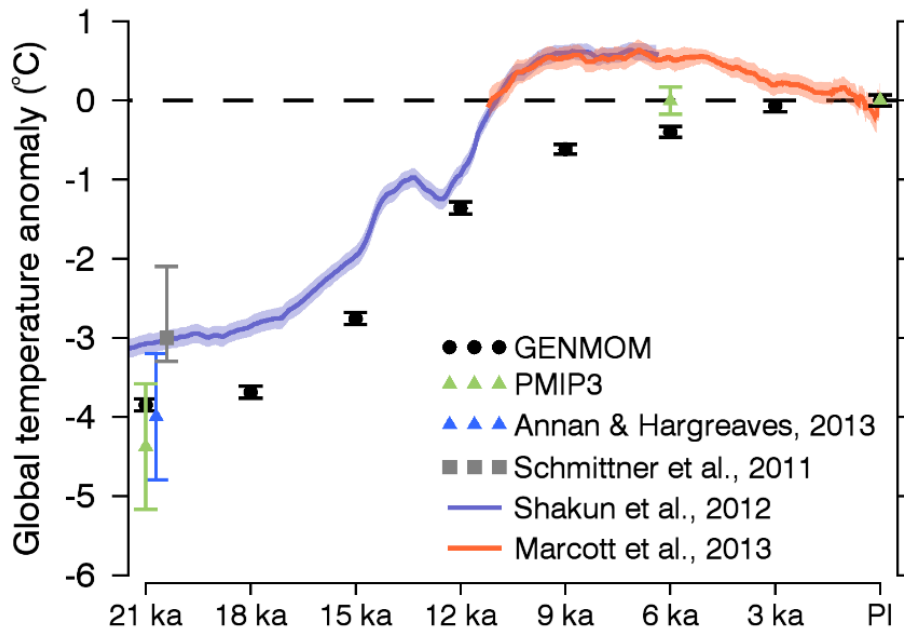


Figure 5. Global surface air temperature (SAT) changes from 21 ka to present. GENMOM is shown as 100 yr averages and standard deviations. The 21 ka and 6 ka PMIP3 data are shown as the ensemble average and its standard deviation. Data-model estimates of mean and range of LGM cooling by Annan and Hargreaves (2013) and Schmittner et al. (2011b). Annan and Hargreaves (2013) and Schmittner et al. (2011b) are offset from 21 ka for legibility. Reconstructions by Shakun et al. (2012) and Marcott et al. (2013) display 1σ uncertainty as a shaded band. Marcott et al. (2013) is adjusted to a pre-industrial (~ 1850) base value rather than the original 1961–1990. Data younger than pre-industrial were removed. The Shakun et al. (2012) and Marcott et al. (2013) time series are joined at their 11.5–6.5 ka means.

Global climate simulations at 3000 year intervals

J. R. Alder and
S. W. Hostetler

Title Page

Abstract

Introduction

Conclusions

References

Tables

Figures

◀

▶

◀

▶

Back

Close

Full Screen / Esc

Printer-friendly Version

Interactive Discussion



Global climate simulations at 3000 year intervals

J. R. Alder and
S. W. Hostetler

Title Page

Abstract

Introduction

Conclusions

References

Tables

Figures



Back

Close

Full Screen / Esc

Printer-friendly Version

Interactive Discussion

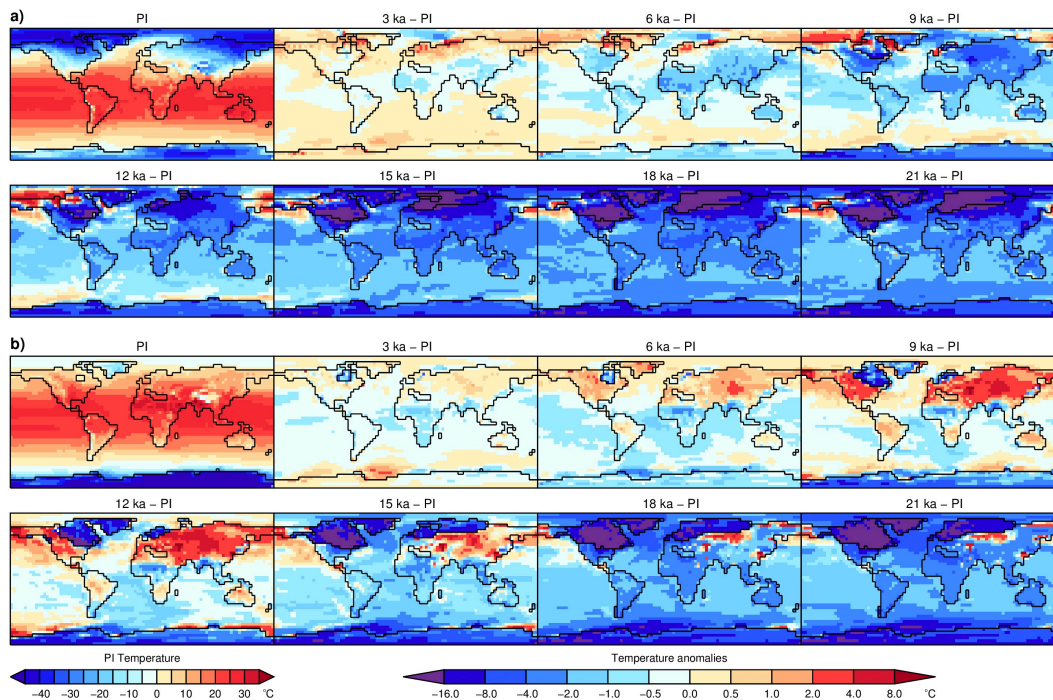


Figure 6. Simulated seasonal average 2 m air temperature anomalies relative to PI. **(a)** December, January, and February and **(b)** June, July, and August.

Global climate simulations at 3000 year intervals

J. R. Alder and
S. W. Hostetler

Title Page

Abstract

Introduction

Conclusions

References

Tables

Figures



Back

Close

Full Screen / Esc

Printer-friendly Version

Interactive Discussion

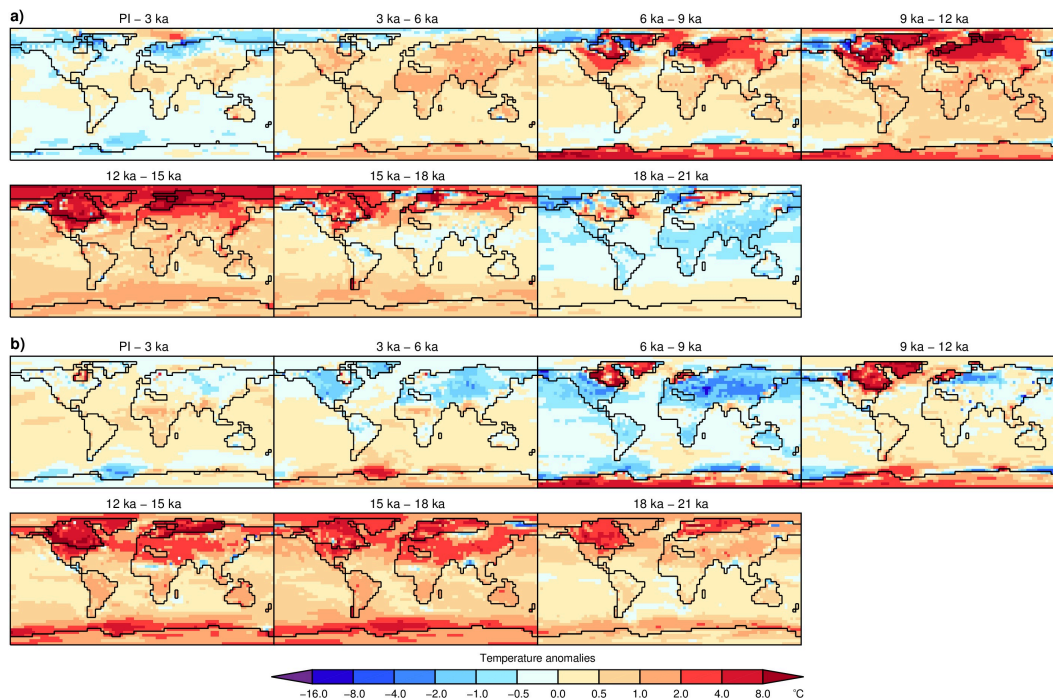


Figure 7. Simulated seasonal average changes in 2 m air between consecutive time segments. **(a)** December, January, and February and **(b)** June, July, and August.

Global climate simulations at 3000 year intervals

J. R. Alder and
S. W. Hostetler

Title Page

Abstract

Introduction

Conclusions

References

Tables

Figures



Back

Close

Full Screen / Esc

Printer-friendly Version

Interactive Discussion

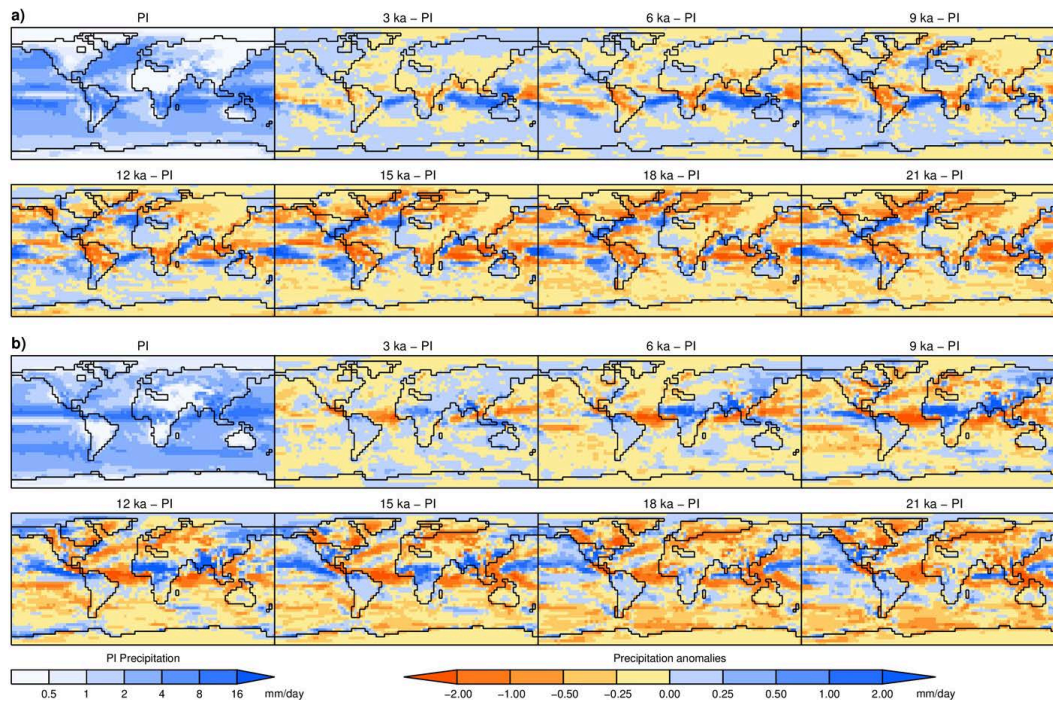


Figure 8. Simulated seasonal average precipitation anomalies relative to PI. **(a)** December, January, and February and **(b)** June, July, and August.

Global climate simulations at 3000 year intervals

J. R. Alder and
S. W. Hostetler

Title Page

Abstract

Introduction

Conclusions

References

Tables

Figures



Back

Close

Full Screen / Esc

Printer-friendly Version

Interactive Discussion

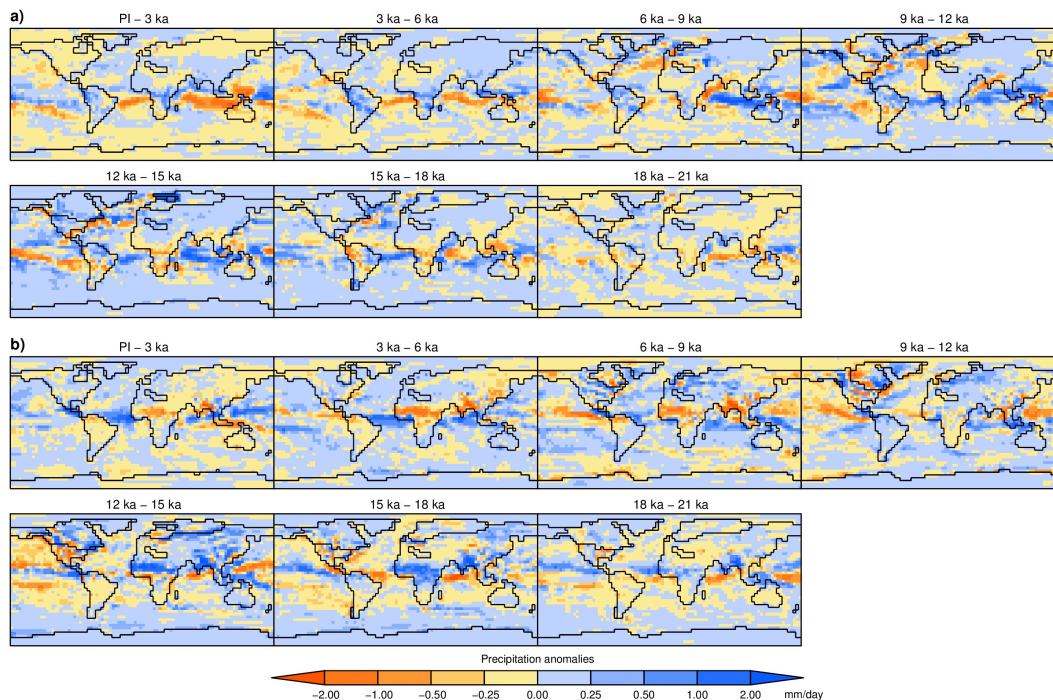


Figure 9. Simulated seasonal average precipitation changes between consecutive time segments. **(a)** December, January, and February and **(b)** June, July, and August.

Global climate simulations at 3000 year intervals

J. R. Alder and
S. W. Hostetler

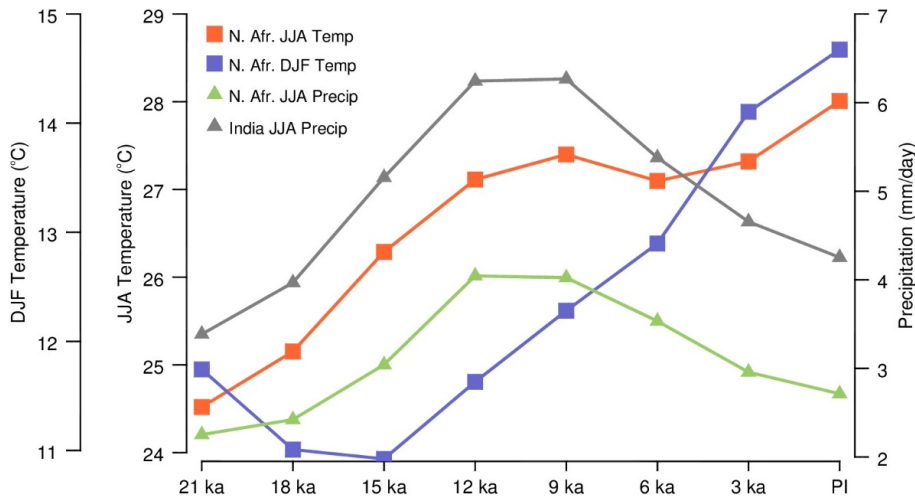


Figure 10. Time evolution of North African and Indian summer monsoons. The North Africa monsoon region is defined as 12–30° N, 20–30° E and India monsoon region is defined as 20–40° N, 70–100° E (Zhao and Harrison, 2012).

Title Page

Abstract

Introduction

Conclusions

References

Tables

Figures



Back

Close

Full Screen / Esc

Printer-friendly Version

Interactive Discussion



Global climate simulations at 3000 year intervals

J. R. Alder and
S. W. Hostetler

[Title Page](#)

[Abstract](#)

[Introduction](#)

[Conclusions](#)

[References](#)

[Tables](#)

[Figures](#)



[Back](#)

[Close](#)

[Full Screen / Esc](#)

[Printer-friendly Version](#)

[Interactive Discussion](#)

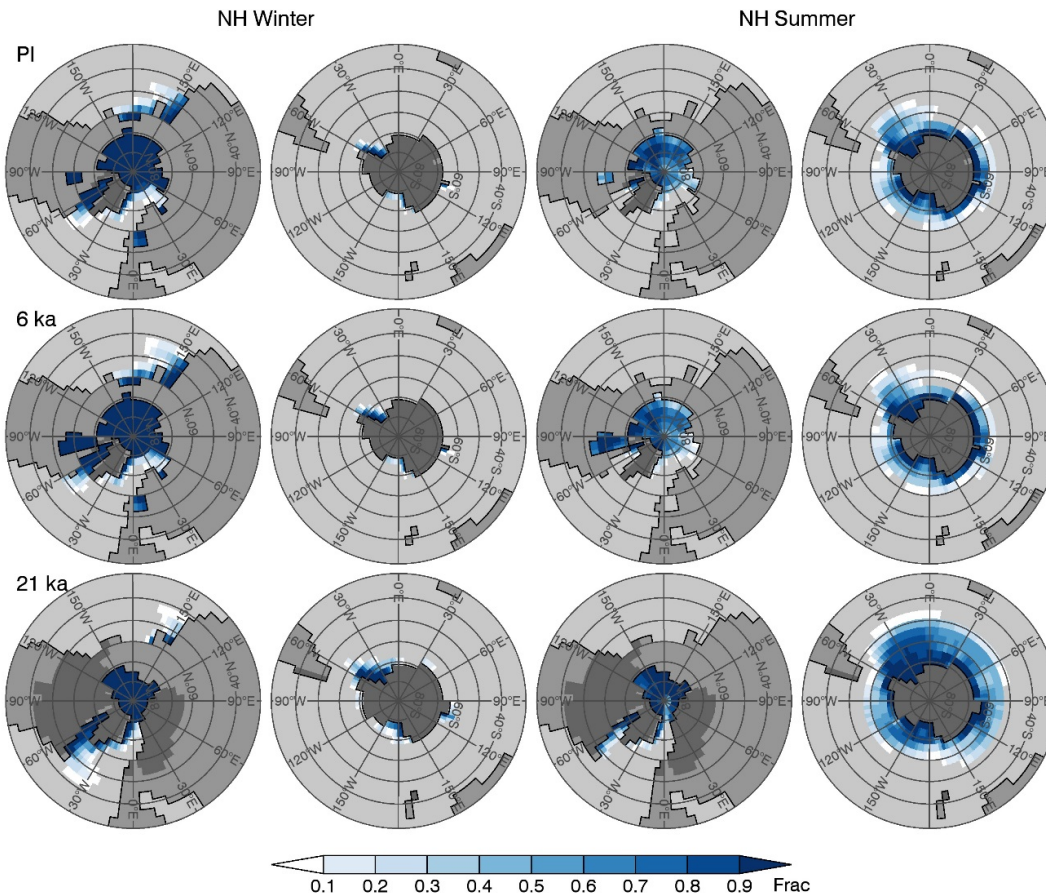


Figure 11. Simulated sea-ice fraction for PI, 6 ka and 21 ka. Left two columns: February–March and right two columns: August–September. Medium gray is continental land mass and dark gray is continental ice sheet.

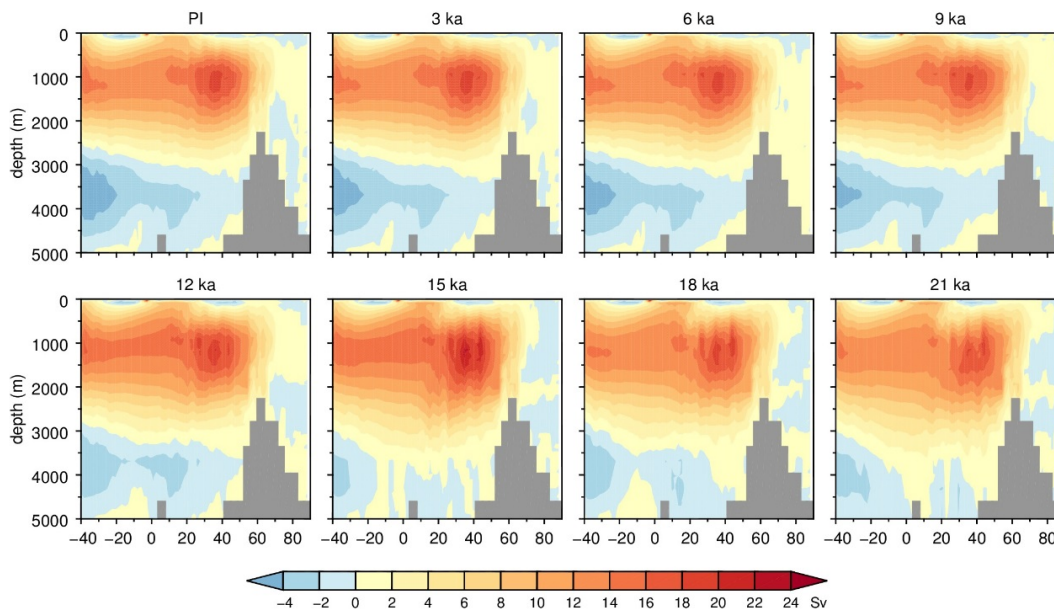
Global climate simulations at 3000 year intervalsJ. R. Alder and
S. W. Hostetler

Figure 12. Simulated annual average Atlantic Meridional Overturning Circulation (AMOC) for the eight time-slices.

[Title Page](#)[Abstract](#)[Introduction](#)[Conclusions](#)[References](#)[Tables](#)[Figures](#)[◀](#)[▶](#)[◀](#)[▶](#)[Back](#)[Close](#)[Full Screen / Esc](#)[Printer-friendly Version](#)[Interactive Discussion](#)

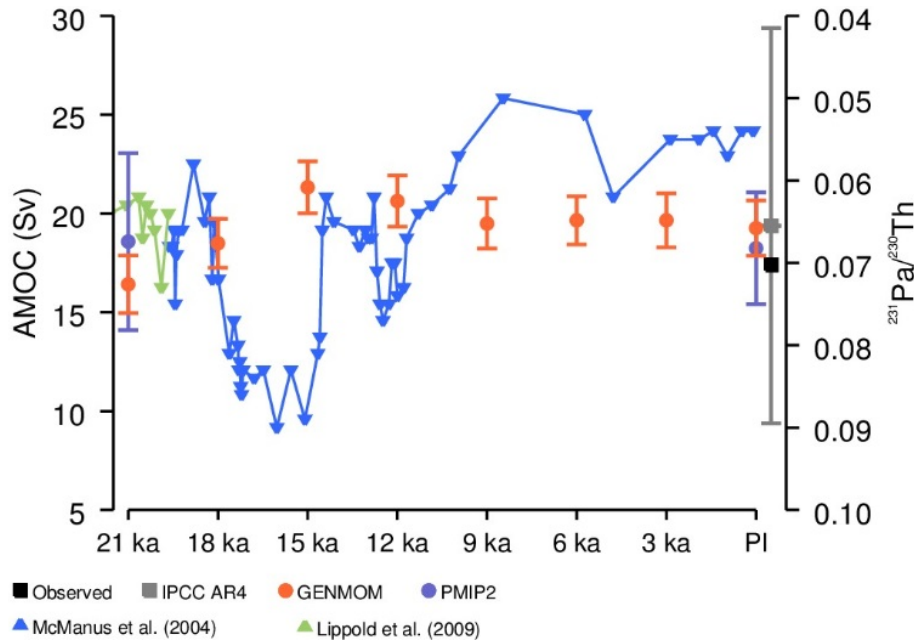


Figure 13. Simulated Atlantic Meridional Overturning Circulation (AMOC) compared to $^{231}\text{Pa}/^{230}\text{Th}$ proxy record at 33°N and other AOGCMs. Observations are from 26.5°N . GENMOM values are 100 yr averages with error bars representing standard deviations. The mean and standard deviation of the maximum AMOC in the five PMIP2 models. The IPCC AR4 point represents the mean and standard deviation from a collection of IPCC AR4 models. $^{231}\text{Pa}/^{230}\text{Th}$ data from McManus et al. (2004) and Lippold et al. (2009); observed value from Srokosz et al. (2012), PMIP2 data from Weber et al. (2007), and IPCC data from Schmittner et al. (2005).

Global climate simulations at 3000 year intervals

J. R. Alder and
S. W. Hostetler

Title Page

Abstract Introduction

Conclusions References

Tables Figures

◀ ▶

◀ ▶

Back Close

Full Screen / Esc

Printer-friendly Version

Interactive Discussion



Global climate simulations at 3000 year intervals

J. R. Alder and
S. W. Hostetler

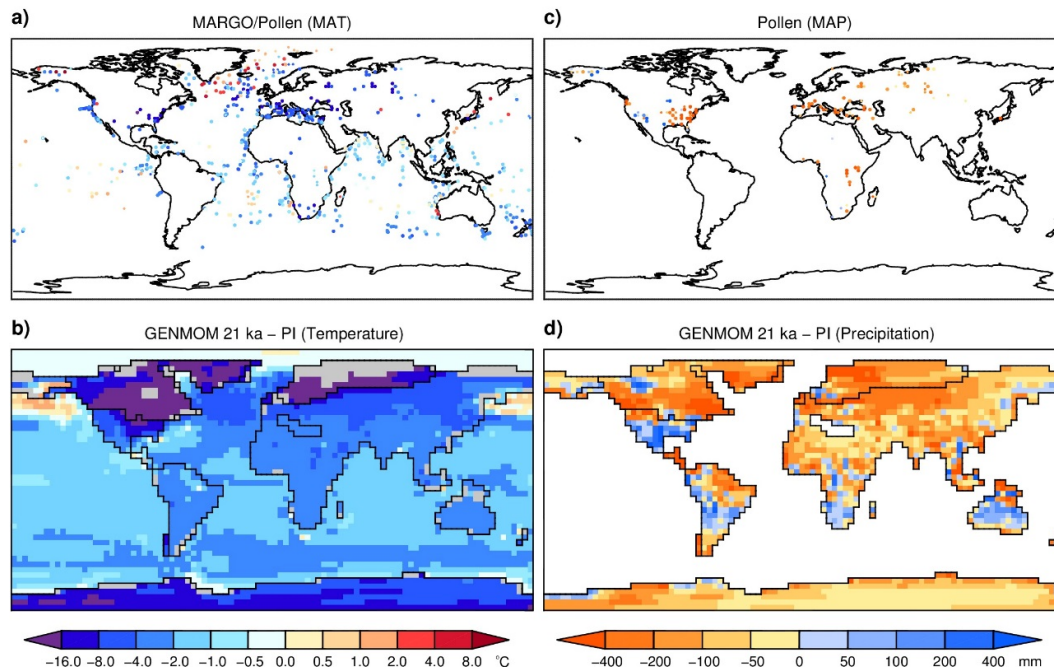


Figure 14. Changes in 21 ka mean annual temperature (MAT) and precipitation (MAP) inferred from data and simulated by GENMOM. **(a)** Blended sea surface temperature from MARGO (Waelbroeck et al., 2009) and terrestrial temperature from Bartlein et al. (2011), **(b)** GENMOM temperature anomalies (blended sea surface temperature and 2 m air temperature over land), **(c)** precipitation from Bartlein et al. (2011), and **(d)** GENMOM precipitation anomalies. Grid cells with different land mask types in the 21 ka and PI simulation are shaded in gray to avoid comparing ocean temperature to land temperature in emergent cells.

Global climate simulations at 3000 year intervals

J. R. Alder and
S. W. Hostetler

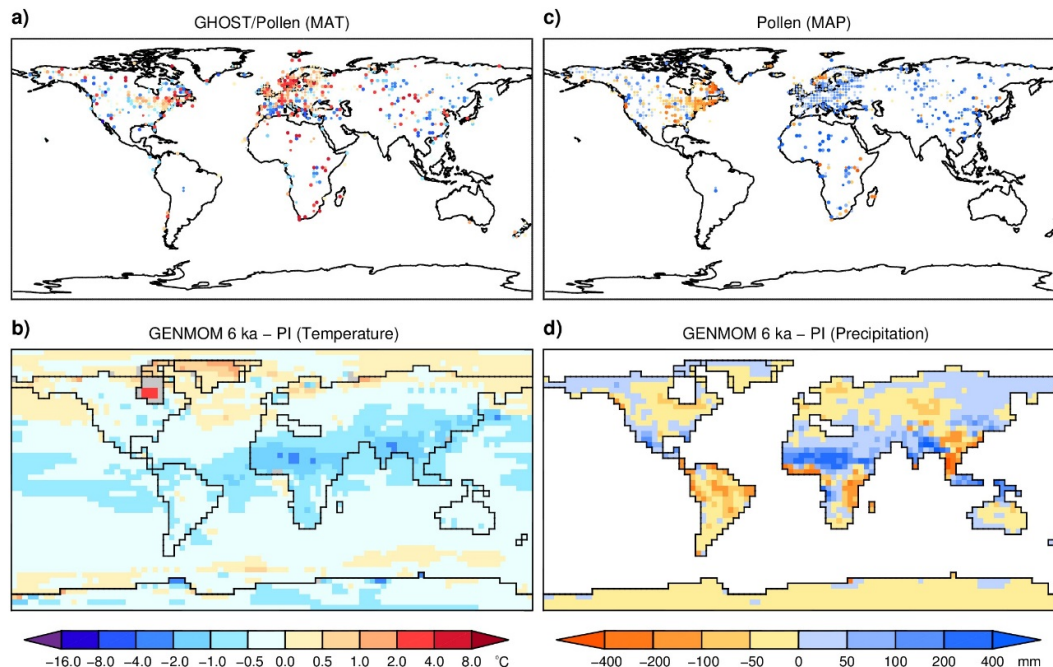


Figure 15. Changes in 6 ka mean annual temperature (MAT) and precipitation (MAP) inferred from data and simulated by GENMOM. **(a)** Blended sea surface temperature from Leduc et al. (2010) and terrestrial temperature from Bartlein et al. (2011), **(b)** GENMOM temperature anomalies (blended sea surface temperature and 2 m air temperature over land), **(c)** precipitation from Bartlein et al. (2011) and **(d)** GENMOM precipitation anomalies. Grid cells with different land mask types in the 6 ka and PI simulation are shaded in gray to avoid comparing ocean temperature to land temperature in emergent cells.

[Title Page](#)
[Abstract](#)
[Introduction](#)
[Conclusions](#)
[References](#)
[Tables](#)
[Figures](#)
[◀](#)
[▶](#)
[◀](#)
[▶](#)
[Back](#)
[Close](#)
[Full Screen / Esc](#)
[Printer-friendly Version](#)
[Interactive Discussion](#)
